© 2017. Published by The Company of Biologists Ltd | Development (2017) 144, 334-344 doi:10.1242/dev.143354

RESEARCH ARTICLE

Osteocrin, a peptide secreted from the heart and other tissues, contributes to cranial osteogenesis and chondrogenesis in zebrafish

Ayano Chiba[1], Haruko Watanabe-Takano[1], Kenta Terai[2], Hajime Fukui[1], Takahiro Miyazaki[1], Mami Uemura[2], Hisashi Hashimoto[3,4], Masahiko Hibi[3,4], Shigetomo Fukuhara[5] and Naoki Mochizuki[1,6,*]

ABSTRACT

The heart is an endocrine organ, as cardiomyocytes (CMs) secrete natriuretic peptide (NP) hormones. Since the discovery of NPs, no other peptide hormones that affect remote organs have been identified from the heart. We identified osteocrin (Ostn) as an osteogenesis/chondrogenesis regulatory hormone secreted from CMs in zebrafish. *ostn* mutant larvae exhibit impaired membranous and chondral bone formation. The impaired bones were recovered by CM-specific overexpression of OSTN. We analyzed the parasphenoid (ps) as a representative of membranous bones. In the shortened ps of *ostn* morphants, nuclear Yap1/Wwtr1-dependent transcription was increased, suggesting that Ostn might induce the nuclear export of Yap1/Wwtr1 in osteoblasts. Although OSTN is proposed to bind to NPR3 (clearance receptor for NPs) to enhance the binding of NPs to NPR1 or NPR2, OSTN enhanced C-type NP (CNP)-dependent nuclear export of YAP1/WWTR1 of cultured mouse osteoblasts stimulated with saturable CNP. OSTN might therefore activate unidentified receptors that augment protein kinase G signaling mediated by a CNP-NPR2 signaling axis. These data demonstrate that Ostn secreted from the heart contributes to bone formation as an endocrine hormone.

KEY WORDS: Osteocrin, Heart, Peptide, Osteogenesis, Chondrogenesis, Nppa, Nppb, Nppc

INTRODUCTION

The heart is not only an essential pump for circulation but also an endocrine organ that secretes natriuretic peptide (NP) hormones, including atrial natriuretic peptide (ANP; also known as NPPA) and brain (B-type) natriuretic peptide (BNP; also known as NPPB) (Ogawa and de Bold, 2014). Cardiomyocytes (CMs) secrete vascular endothelial growth factor A and angiopoietin 1 to direct coronary vascular development in a paracrine-dependent manner by acting on endothelial cells during cardiogenesis (Arita et al., 2014; Riley and Smart, 2011). Therefore, CMs have the potential to secrete functional peptides, although the main function of CMs is in cardiac muscle contraction. Besides ANP and BNP, no other secretory peptides that function as endocrine hormones have been reported.

The NP family consists of ANP, BNP and C-type NP (CNP; also known as NPPC). These NPs bind to the NPR1, NPR2 and NPR3 family of transmembrane receptors. NPR1 and NPR2 have a guanylate cyclase domain, whereas NPR3 does not. NPR3 functions as a clearance receptor for ANP and BNP or as a Gi-activating receptor (Potter et al., 2006). ANP induces natriuresis in the kidney and relaxation of smooth muscle via NPR1 and NPR2. ANP exerts paracrine/autocrine roles on CMs in the heart, as ANP has recently been reported to regulate CM proliferation in zebrafish (Becker et al., 2014). In contrast to ANP and BNP, CNP is produced in a variety of tissues and organs including the uterus, ovarium, cartilaginous tissues, blood vessels and osteoblasts (Hagiwara et al., 1994; Stepan et al., 1999, 2002; Suda et al., 1996). It characteristically elongates long bones through NPR2 expressed on chondrocytes. The physiological relevance of CNP-NPR2 signaling to bone formation is apparent because *Cnp* (*Nppc*) knockout mice and *Npr2* knockout mice exhibit dwarfism (Komatsu et al., 2002; Tamura et al., 2004). Conversely, the forced expression of CNP and the depletion of *Npr3* result in increased bone length in mice (Dauphinee et al., 2013; Kake et al., 2009; Matsukawa et al., 1999).

Bone growth depends on endochondral ossification and intramembranous ossification (Karsenty et al., 2009). The former occurs during growth of the long bones, whereas the latter is found in the calvaria and clavicle. The chondrocyte lineage cells – prechondrogenic cells, proliferating chondrocytes, prehypertrophic chondrocytes and hypertrophic chondrocytes – participating in endochondral ossification respond to BNP and CNP because they express NPR2 receptors (Suda et al., 1998; Yasoda et al., 2004). Therefore, enhancement of BNP/CNP-NPR2 signaling results in the extension of long bones. During intramembranous ossification, osteoblasts differentiated from mesenchymal stem cells (MSCs) proliferate and secrete bone matrix, thereby contributing to bone formation in a manner that is independent of chondrocytes (Soltanoff et al., 2009).

Osteocrin (OSTN) is proposed to belong to the NP family as there are similarities in amino acid sequence (Moffatt and Thomas, 2009; Potter et al., 2006). OSTN and musclin were originally identified by signal-sequence trap methods as the same molecule from bone and muscle, respectively (Nishizawa et al., 2004; Thomas et al., 2003). The C-terminus of OSTN seems to be cleaved at 76KKKR79 and 110KKR112 sites. The resulting two fragments OSTN80-109 and OSTN113-130 have amino acid homology to NPs (Moffatt and Thomas, 2009), although neither fragment has the Cys-Cys

[1]Department of Cell Biology, National Cerebral and Cardiovascular Center Research Institute, 5-7-1 Fujishirodai, Suita, Osaka 565-8565, Japan. [2]Laboratory of Function and Morphology, Institute of Molecular and Cellular Biosciences, University of Tokyo, 1-1-1 Yayoi, Bunkyo-ku, Tokyo 113-0032, Japan. [3]Laboratory of Organogenesis and Organ Function, Bioscience and Biotechnology Center, Nagoya University, Furo-cho, Chigusa-ku, Nagoya, Aichi 464-8061, Japan. [4]Devision of Biological Science, Graduate School of Science Nagoya, Nagoya University, Furo-cho, Chigusa-ku, Nagoya, Aichi 464-8061, Japan. [5]Department of Molecular Pathophysiology, Institute of Advanced Medical Science, Nippon Medical School, 1-396 Kosugi-machi, Nakahara-ku, Kawasaki, Kanagawa 211-8533, Japan. [6]AMED-CREST, National Cerebral and Cardiovascular Center Research Institute, 5-7-1 Fujishirodai, Suita, Osaka 565-8565, Japan.

*Author for correspondence (nmochizu@ri.ncvc.go.jp)

N.M., 0000-0002-3938-9602

Received 5 August 2016; Accepted 28 November 2016

Development (2017) 144, 334-344 doi:10.1242/dev.143354

signature that is conserved in NPs and is essential for their circular structure. Nonetheless, OSTN is capable of binding to NPR3, thereby hampering the NP clearance activity of NPR3 (Thomas et al., 2003). Consistent with these findings, *Ostn* transgenic (Tg) mice exhibit extended long bones and kyphosis, presumably owing to the activation of NPR2 found in *Bnp* (*Nppb*) Tg mice (Suda et al., 1998; Thomas et al., 2003). The physiological role of OSTN in osteogenesis remains unclear, although it has been shown utilizing *Ostn* knockout mice to function as a myokine (Subbotina et al., 2015).

In this study, we aimed to search for secretory peptides from CMs of zebrafish and identified Ostn derived from the heart as an endocrine regulator for bone and cartilage. Ostn depletion led to shortening of the parasphenoid (ps), which is regulated by intramembranous ossification, and of the palatoquadrate (pq), which is regulated by chondrogenesis, while Ostn overexpression resulted in elongation of ps and pq. We further investigated how Ostn regulates ps formation, and found that Ostn regulates bone/cartilage formation by modifying CNP-dependent nuclear export of the transcriptional co-factors Yap1 and Wwtr1.

RESULTS

Ostn is expressed in CMs

ANP and BNP produced in the heart induce natriuresis through activation of NP receptors expressed in the renal tubules. Thus, the heart is thought to be an endocrine organ. First, we searched for secretory peptides produced from the heart. To obtain only CMs from the heart, we established two Tg zebrafish (*Danio rerio*) lines: *Tg(myl7:NLS-mCherry)* and *Tg(myl7:actn2-tdEos)* (Fig. 1A,C, Movies 1 and 2). Both the nuclear localization signal (NLS)-tagged monomeric (m)Cherry and actinin alpha 2 (Actn2)-tandem (td) Eos were seen to be exclusively expressed in the CMs using the *cardiac myosin light chain* (*myl7*) promoter when we carefully observed the fluorescence in heart by lightsheet and confocal microscopy. We isolated CMs from the hearts of these two Tg lines by fluorescence-activated cell sorting (FACS). *ostn* mRNA was expressed in the CMs of larvae of both Tg lines at 72 h post-fertilization (hpf) (Fig. 1B,D). The expression of mRNAs from the CMs was validated by the expression of *nppa*, *myl7* and *actc1a*. Moreover, genes known to be expressed in CMs, including *angpt1*, *bmp1a* and *epo*, were detected by RNA-seq (Fig. 1B,D).

We then examined the expression of *ostn* mRNA by whole-mount *in situ* hybridization (WISH) of larvae at 72 hpf. *ostn* mRNA was detected in the heart, corpuscles of Stannius (CS) and head (Fig. 2A). *ostn* mRNA was expressed in the heart where *myl7* mRNA was detected. Moreover, the expression of *ostn* mRNA seemed to be greater in the ventricle than in the atrium (Fig. 2B). The expression of *ostn* mRNA in the CS was confirmed by WISH of *calcium-sensing receptor* (*casr*) (Lin et al., 2014). Although *ostn* mRNA was exclusively expressed in the heart and CS at 36 hpf, it began to be detected in the head at 72 hpf (Fig. 2B). We examined in detail this expression in the head in brain sections to see whether it overlaps with that of myocytes (*myod1*), osteoblasts (*sp7*) and chondrocytes (*sox9a*). We found no clear overlap between *ostn* expression and these marker genes (Fig. S1). In addition, we investigated *Ostn* expression in adult mice (*Mus musculus*) and embryos by reverse transcription (RT)-PCR. *Ostn* mRNAs were mainly expressed in bones and muscles in adult mice, whereas subtle expression was detected in both atrium and ventricle of the embryonic mouse heart (Fig. S2A,B). These data suggest the possibility that Ostn secreted from CMs of zebrafish might function as a hormone that affects remote organs, including bones during early embryogenesis, just as mouse OSTN affects bone formation (Moffatt et al., 2007).

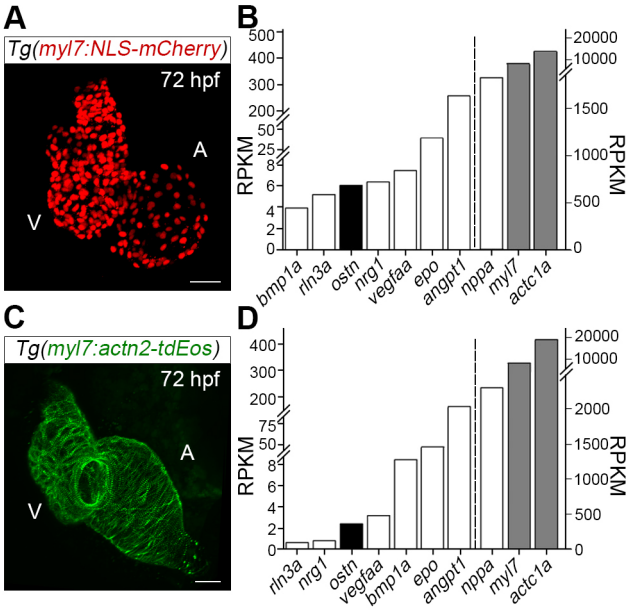

Fig. 1. Osteocrin (Ostn) is produced in cardiomyocytes of zebrafish. (A) Projection view of confocal images of the *Tg(myl7:NLS-mCherry)* heart at 72 hpf. A, atrium; V, ventricle. (B) RNA-seq analyses of mCherry-positive cardiomyocytes (CMs) from the hearts of *Tg(myl7:NLS-mCherry)* larvae at 72 hpf. Left and right *y*-axes report RPKM (reads per kilobase per million sequenced reads) values for the secretory molecules (left of the dashed line) and positive controls (right of the dashed line), respectively. Gray bars are used for structural proteins, white bars for secretory molecules. (C) Projection view of confocal images of the *Tg(myl7:actn2-tdEos)* heart at 72 hpf. (D) RNA-seq analyses of tdEos-positive CMs of *Tg(myl7:actn2-tdEos)*. Axes descriptions as in B. Scale bars: 30 µm.

Ostn derived from CMs contributes to membranous bone formation

To study the function of Ostn in zebrafish osteogenesis, we developed *ostn* knockout fish using transcription activator-like effector nuclease (TALEN). TALEN targeting to *ostn* successfully

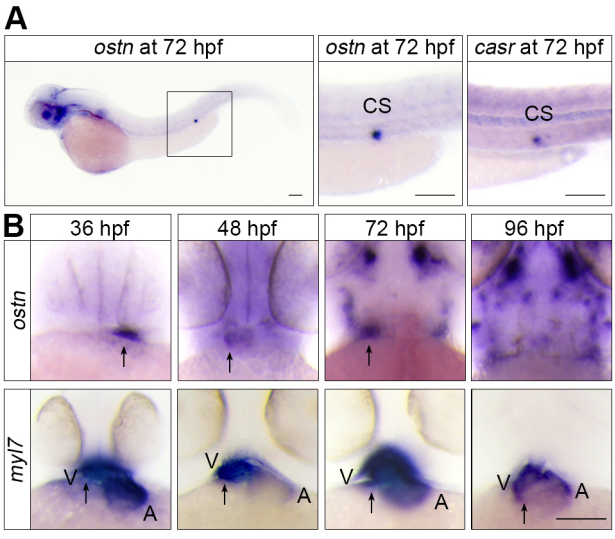

Fig. 2. Ostn is expressed in the ventricle of hearts and corpuscles of Stannius. (A) Whole-mount *in situ* hybridization (WISH) analyses of *ostn* mRNA expression in a zebrafish larva at 72 hpf (left), and *ostn* (middle) and *casr* (right) mRNA expression at corpuscles of Stannius (CS). (B) WISH analyses of *ostn* and *myl7* mRNAs of larvae at the indicated time points. Arrows indicate the ventricles. A, atrium; V, ventricle. Scale bars: 100 µm.

Development (2017) 144, 334-344 doi:10.1242/dev.143354

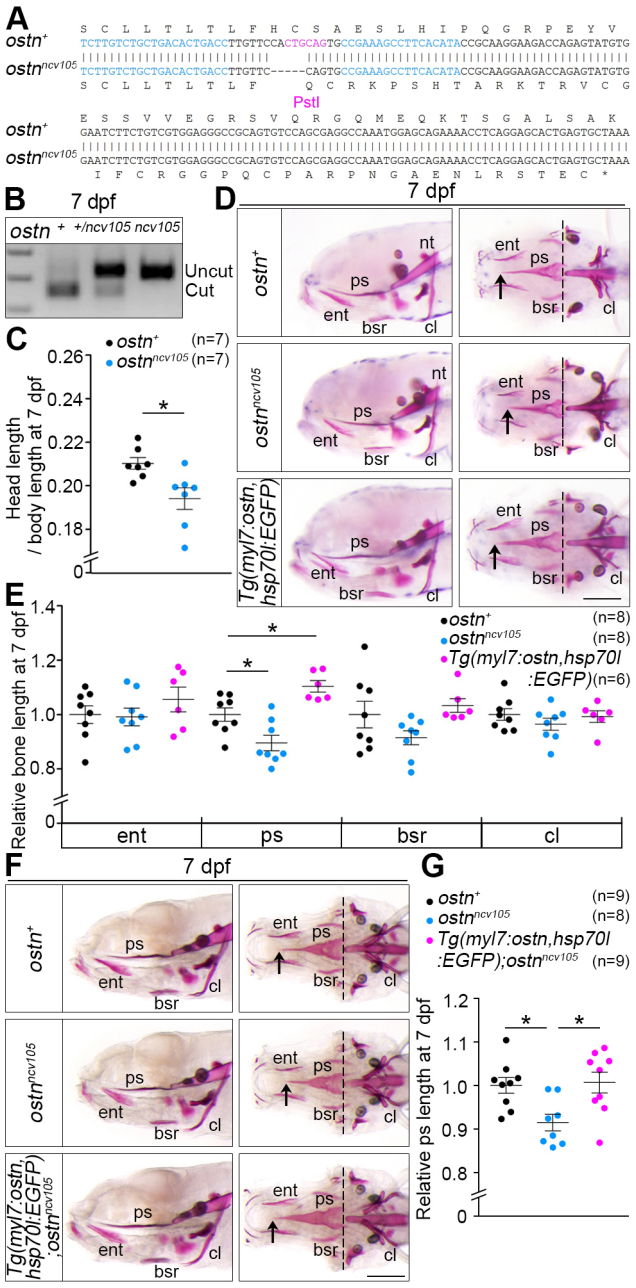

Fig. 3. Depletion and overexpression of Ostn result in shortening and elongation, respectively, of the parasphenoid at an early stage. (A) DNA and corresponding amino acid sequence of the *ostn*^{ncv105} allele. The 5 bp deletion in *ostn*^{ncv105} leads to the mutation of 40 amino acids followed by a premature termination (asterisk). (B) Genotype of wild-type (+), heterozygous (*+/ncv105*) and homozygous (*ncv105*) alleles as confirmed by digestion of PCR products containing a *Pst*I site as indicated in A. (C) Ratio of head length [from the tip of the upper jaw to the caudal part of the Alizarin Red stained notochord (nt)] to body length (from the tip of the upper jaw to the end of the tail) of 7 dpf wild-type (+) or homozygous mutant (*ncv105*) larvae. Each point indicates data from an individual larva. *n*, number of larvae examined. (D) Representative images of Alizarin Red staining of 7 dpf larvae of wild type (top), *ostn*^{ncv105} homozygous mutant (middle) and *Tg(myl7:ostn,hsp70l:EGFP)* (bottom). Lateral view (left) and ventral view (right), anterior to the left. Arrows and dashed lines indicate the tip and the top of the concave in the caudal part of the parasphenoid (ps), respectively. (E) Quantitative analyses of cranial bone length of 7 dpf *ostn*^{ncv105} and transgenic larvae relative to the mean length of wild-type bones is plotted for entopterygoid (ent), ps (between arrow and dashed line in D), branchiostegal ray (bsr) and cleithrum (cl). (F) Representative images of Alizarin Red staining of 7 dpf larvae of wild type (top), *ostn*^{ncv105} homozygous mutant (middle) and *Tg(myl7:ostn,hsp70l:EGFP);ostn*^{ncv105}. Views as in D. (G) Quantitative analyses of F. Data were analyzed by Student's *t*-test or one-way ANOVA with Tukey's test. **P*<0.05. Error bars indicate s.e.m. Scale bars: 200 µm.

deleted 5 bp. The resulting allele encoded 40 mutated amino acids from Phe18 (F), followed by a premature termination codon (Fig. 3A). We named these mutants *ostn*^{ncv105} and screened them by genomic PCR product digestion with *Pst*I (Fig. 3A,B). We also developed the *Tg(myl7:ostn,hsp70l:EGFP)* line, in which Ostn is expressed exclusively in the heart, to investigate the effect of overexpression of Ostn on bone formation.

Shortened heads were apparent in *ostn*^{ncv105} larvae (Fig. 3C, D). We further examined the length of the head and body during development from embryo and larva. Significant shortening of head length was first observed at 6 days post-fertilization (dpf), when the growth of bones and cartilage became active (Fig. S3A, B). We quantitatively measured the ratio of head length to total body length and the length of cranial bones: entopterygoid (ent), parasphenoid (ps), branchiostegal ray (bsr) and cleithrum (cl). Head length was shorter in the mutant than in the control at 7 dpf. Whereas the ps was shorter in *ostn*^{ncv105} than in wild-type larvae, other intracranial membranous bones (ent, bsr and cl) were comparable in length among *ostn*^{ncv105} mutants, *Tg(myl7:ostn,hsp70l:EGFP)* and wild-type larvae at 7 dpf (Fig. 3D,E). Head length of *ostn*^{ncv105} larvae remained shorter than in the control at 10 dpf (Fig. S4A). Consistently, the length of all the cranial bones in *ostn*^{ncv105} larvae was now shorter than in control larvae (Fig. S4B,C).

Next, we examined the effect of *ostn* knockdown using morpholino oligonucleotides (MOs) on the length of the ps. In *ostn* morphants, the ps was shorter than in larvae injected with vehicle (Fig. S4D-F). We confirmed that the circulation was unaffected in the *ostn* morphants (Movies 3 and 4).

To further examine the contribution of Ostn derived from CMs to bone formation, we crossed the *Tg(myl7:ostn,hsp70l:EGFP)* and *ostn*^{ncv105} fish. The shortened ps found in *ostn*^{ncv105} larvae was reversed by the overexpression of Ostn in CMs (Fig. 3F,G). These data suggest that Ostn derived from CMs might contribute to bone formation.

Ostn contributes to endochondral bone formation

We then explored the contribution of Ostn to endochondral bone formation, measuring the length of pharyngeal cartilages, ethmoid plate (ep), trabeculae (tr), Meckel's cartilage (mc), palatoquadrate (pq) and hyosymplectic (hs) in *ostn*^{ncv105} larvae (Schilling and Kimmel, 1997). The mc and pq were shorter in the mutant than in the control (Fig. 4A,B). In clear contrast, the ps and hs were longer in *Tg(myl7:ostn,hsp70l:EGFP)* than in the control. In addition, all except tr were longer in *Tg(myl7:ostn,hsp70l:EGFP)* than in *ostn*^{ncv105} larvae.

We attempted to understand the reason why these bones were shortened in the mutant larvae and elongated in larvae overexpressing Ostn. The area of the pq, in which the pterygoid process (pp) was excluded, was smaller in the mutant than in the control (Fig. 4C,D), whereas it was larger in *Tg(myl7:ostn,hsp70l:EGFP)* larvae. We then counted the number and measured the area of individual chondrocytes including extracellular matrix in the pq (Fig. 4C,E,F). Although the number of cells was comparable between mutant and control, the area of individual chondrocytes was smaller in *ostn*^{ncv105} larvae and greater in *Tg(myl7:ostn,hsp70l:*

Development (2017) 144, 334-344 doi:10.1242/dev.143354

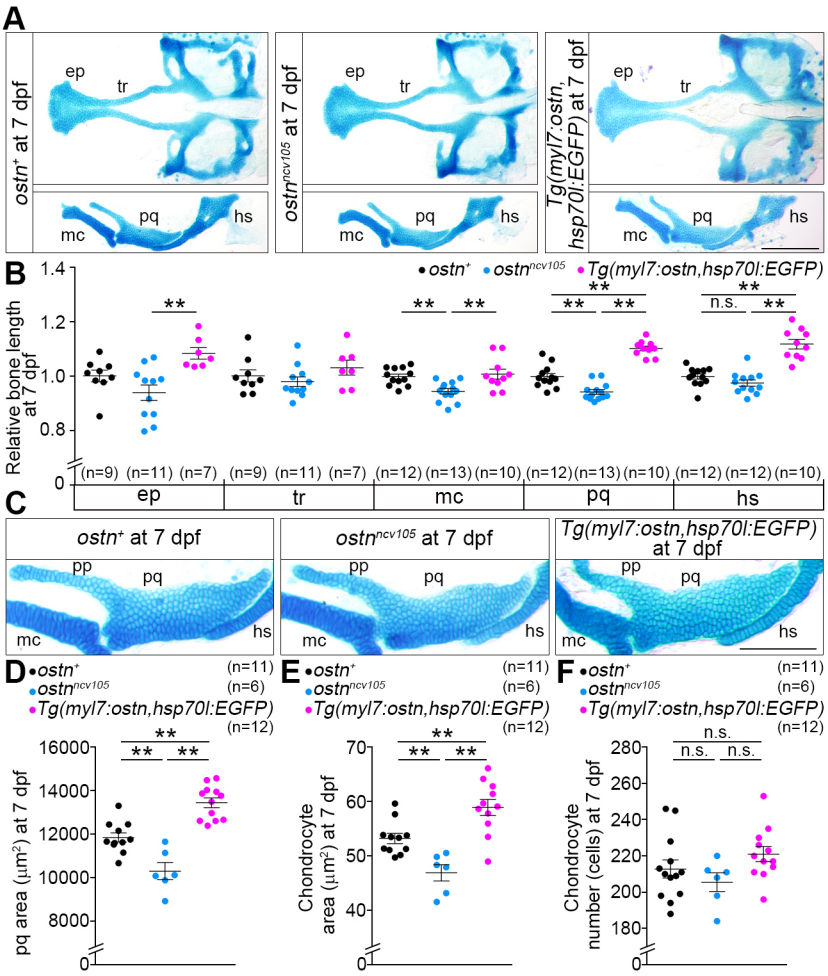

Fig. 4. Ostn regulates the growth of endochondral bone formation. (A) Representative images of Alcian Blue staining of cranial cartilages of a wild-type (*ostn*$^{+}$; left), *ostn*^{ncv105} mutant (center) and Ostn-overexpressing [right; *Tg(myl7:ostn,hsp70l:EGFP)*] larva at 7 dpf. ep, ethmoid plate; tr, trabeculae; mc, Meckel's cartilage; pq, palatoquadrate; hs, hyosymplectic. (B) Quantitative analyses of A. Bone length relative to the mean length of wild-type bones is plotted. (C) Representative images of Alcian Blue staining of cartilages of the lower jaw of a wild-type, *ostn*^{ncv105} mutant and Ostn-overexpressing larva at 7 dpf. pp, pterygoid process. (D) Quantitative analyses of the area of the ps of wild-type, *ostn*^{ncv105} mutant and Ostn-overexpressing larvae at 7 dpf. (E) Quantitative analyses of the area of individual chondrocytes in the pq. (F) The number of chondrocytes in the pq. $^{**}P<0.01$; n.s., no significant difference between two groups. Error bars indicate s.e.m. Scale bars: 200 µm in A; 100 µm in C.

EGFP) larvae than in the control, suggesting that Ostn might be involved in the regulation of endochondral bone formation.

Collectively, our data indicate the contribution of Ostn to both membranous and endochondral bone formation.

Ostn affects Yap1- or Wwtr1-dependent transcriptional regulation in the parasphenoid

The ps develops according to intramembranous ossification that requires the maturation of MSCs to osteoblasts. Runx2 is an essential transcription factor promoting the differentiation of MSCs to preosteoblasts (Komori et al., 1997; Long and Ornitz, 2013). Sp7 (osterix) is required for preosteoblast differentiation to mature osteoblasts (Zhou et al., 2010). We examined the promoter activity of these two essential transcription factors.

To observe *runx2* promoter-dependent transcription and *sp7* promoter-dependent transcription, respectively (Knopf et al., 2011; Spoorendonk, et al., 2008), we developed two Tg lines: *Tg(Hsa.RUNX2:GAL4FF-2A-mCherry)* in which GAL4FF is expressed under the human (*Homo sapiens*) *RUNX2* promoter; and *Tg*(*Ola.sp7:GAL4FF-2A-mCherry)* in which GAL4FF is expressed under the medaka fish (*Oryzias latipes*) *sp7* promoter. These Tg lines were crossed with *Tg(UAS:EGFP)* and expression of the EGFP reporter compared with that of endogenous *runx2a/b* and *sp7* mRNAs (Fig. S5A,B). EGFP reporter expression in *Tg(Hsa.RUNX2:GAL4FF-2A-mCherry);(UAS:EGFP)* or *Tg*(*Ola.sp7:GAL4FF-2A-mCherry);(UAS:EGFP)* overlapped with the expression domains of endogenous *runx2a/b* or *sp7* mRNA as detected by WISH, indicating that these Tg fish can be used to monitor *runx2* and *sp7* promoter activity. We compared EGFP fluorescence in larvae injected with vehicle with that of *ostn* morphants. Fluorescence intensity of the ps was comparable in *ostn* morphant and control larvae (Fig. 5A), indicating that *runx2* and *sp7* promoter activity is unaffected by Ostn.

The function of YAP1 and WWTR1 (TAZ) in osteogenesis has been controversial. YAP1 represses RUNX2-mediated transcription (Zaidi et al., 2004). WWTR1 functions as a coactivator for RUNX2 during MSC differentiation to osteoblast (Hong et al., 2005), while osteoblast-specific overexpression of WWTR1 enhances bone formation (Yang et al., 2013). We monitored Yap1/Wwtr1 transcriptional activity in zebrafish using *Tg(Ola.sp7:Gal4db-Hsa.TEAD2ΔN-2A-mCherry);(UAS:EGFP)* larvae, in which nuclear translocated Yap1 or Wwtr1 induces GAL4/UAS system-driven EGFP expression (Fig. 5B). When *ostn* was knocked down by MO, Yap1/Wwtr1-dependent transcription was increased (Fig. 5C,D), suggesting that nuclear translocation of Yap1/Wwtr1 is suppressed by Ostn-mediated signaling. Consistent with the results that there was no difference of bone length except the ps in *ostn* mutants at 7 dpf (Fig. 3E), Yap1-dependent transcription in the op, bsr and ent at 6 dpf was comparable between *ostn* morphants and control (Fig. S8A,B).

To test whether Yap1 regulates growth of the ps, we overexpressed the constitutively active form Yap1-5SA or the dominant-negative Yap1-Tead interfering peptide (Ytip) (von et al., 2012; Zhao et al., 2007). Larvae expressing Yap1-5SA were selected by *crystallin alpha*

Development (2017) 144, 334-344 doi:10.1242/dev.143354

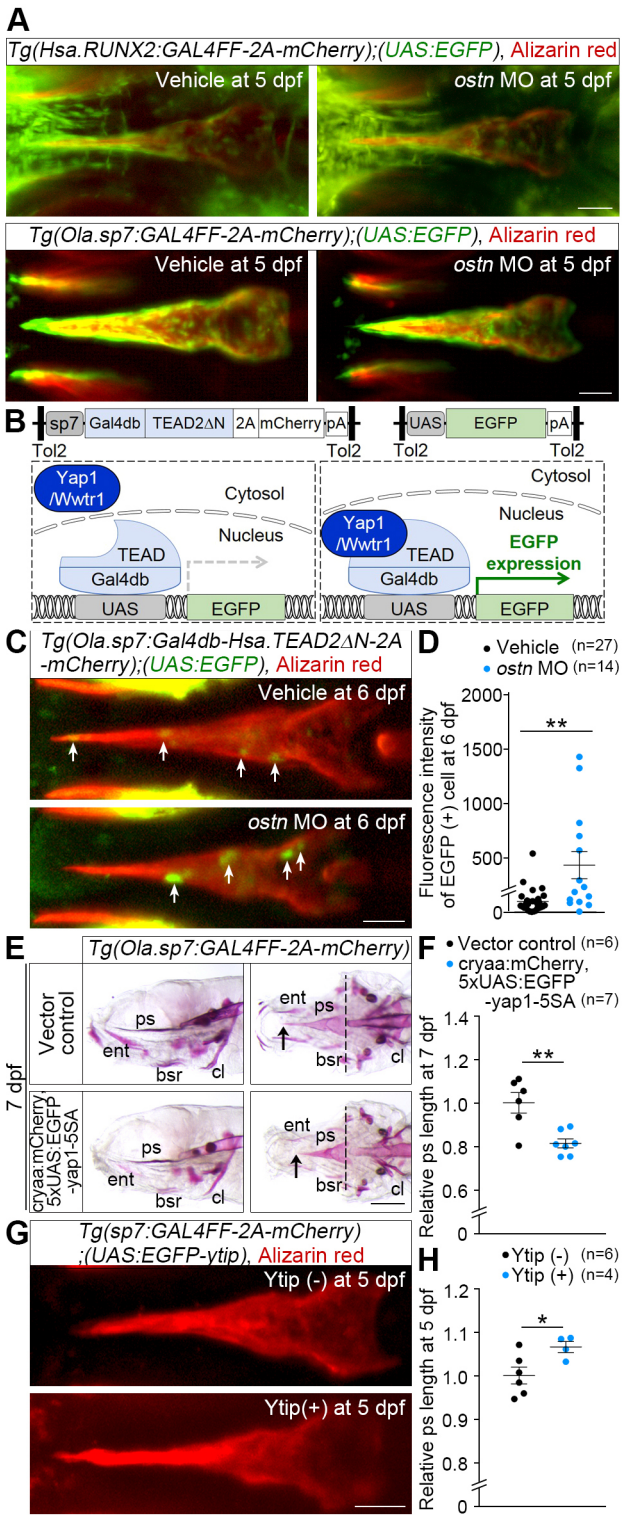

Fig. 5. Ostn regulates osteogenesis through Yap1/Wwtr1. (A) *runx2* and *sp7* promoter activity monitored by EGFP in the ps of *Tg(Hsa.RUNX2:GAL4FF-2A-mCherry);(UAS:EGFP)* larvae (top) and those of *Tg(Ola.sp7:Gal4FF-2A-mCherry);(UAS:EGFP)* (bottom) treated with vehicle (left) or *ostn* MO (right). Confocal images are of larvae stained with Alizarin Red at 5 dpf. (B) Illustration of how Tg fish enable detection of nuclear translocation of Yap1/Wwtr1 by EGFP expression in tissues where the *sp7* promoter is active. (C) Confocal images of the ps of Tg larvae injected with vehicle (top) or *ostn* MO (bottom) and stained with Alizarin Red at 6 dpf. Arrows indicate EGFP-positive cells, which correspond to those in which Yap1/Wwtr1 enter the nucleus. (D) Quantitative analysis of C. The intensity of the EGFP-positive area in the ps is plotted. The number of EGFP-positive areas quantified is indicated at the top. (E) Representative images of Alizarin Red staining of *Tg(Ola.sp7:Gal4FF-2A-mCherry)* larvae at 7 dpf transiently transfected with the plasmids indicated on the left. Lateral view (left) and ventral view (right), anterior to the left. Arrows and dashed lines indicate the tip and the top of concave of the caudal part of the ps, respectively. (F) Quantitative analyses of ps length of the larvae in E. The length of ps was measured as in Fig. 3E. (G) Representative images of Alizarin Red staining of the ps of *Tg(Ola.sp7:GAL4FF-2A-mCherry); (UAS:EGFP-ytip)* larvae at 5 dpf. (H) Quantitative analyses of G. ps length relative to the mean length of the wild-type ps was plotted. **P*<0.05, ***P*<0.01. Error bars indicate s.e.m. Scale bars: 50 µm in A,C,G; 200 µm in E.

A (*cryaa*) promoter-driven mCherry expression in the eyes. When Yap1-5SA was transiently expressed using the *sp7* promoter and GAL4/UAS system, the ps became shortened (Fig. 5E,F). In clear contrast, when Ytip was stably expressed in the ps using the GAL4/UAS system, the ps became elongated (Fig. 5G,H). These data suggest that Ostn-dependent inhibition of a Yap1-mediated signal is involved in the growth of the membranous bones.

Yap1 is known to regulate cell proliferation, apoptosis and differentiation (Varelas, 2014; Zhao et al., 2010). Therefore, we examined the differentiation of preosteoblasts and osteoblasts by the expression of *runx2a/b*, *sp7* and *spp1* mRNAs in *ostn*^{ncv105} mutant larvae. The expression of these genes was comparable between mutant and control larvae (Fig. S6A-D). Furthermore, we analyzed cell proliferation and apoptosis in the ps of *ostn* morphants and control. When the proliferation of ps cells marked by EGFP was analyzed by EdU incorporation, we found no difference between the two groups (Fig. S7A,C). Using another Tg fish, *Tg(Ola.sp7:EGFP)*, to directly mark cells in the ps, TUNEL staining revealed that apoptotic cells were barely or undetected in the ps of *ostn* morphant or control larvae (Fig. S7B,D). In addition, we investigated the maturation of osteoblasts and chondrocytes by the expression of *col10a1* mRNA, which is known to be inhibited by Yap1 (Deng et al., 2016). There was no significant difference in *col10a1* expression between control and *ostn*^{ncv105} larvae when examined at 4 dpf by WISH (Fig. S6E). However, when examined by quantitative (q)RT-PCR, *col10a1* mRNA expression was suppressed in *ostn*^{ncv105} larvae at 7 dpf (Fig. S6F,G).

Since *ctgfa* gene expression is promoted by Yap1 and Wwtr1 (Zhang et al., 2009; Zhao et al., 2008), we examined whether Ctgfa is involved in ps growth. When Ctgfa was overexpressed, the ps was shortened (Fig. S8C,D). By contrast, the ps of *ctgfa* morphants tended to be longer than in control morphants (Fig. S8E,F), although the difference was not significant. In addition, we confirmed the expression of *ctgfa* mRNA in the ps of control larvae (Fig. S13D), suggesting the participation of Ctgfa in ps growth. We assume that the reason why there was no significant difference in ps length between *ctgfa* morphants and control morphants is because the *ctgfa* morphants exhibiting cardia bifida, in which the expression of *ctgfa* mRNA was greatly reduced, were excluded from this analysis. These data suggest that the Yap1-Ctgfa signaling induces shortening of the ps, whereas Ostn induces elongation of the ps. These data for membranous bone growth and the data for cartilage growth suggest that Ostn contributes to growth of bones not by regulating proliferation, apoptosis or differentiation, but presumably by regulating bone matrix via a Ctgfa-dependent signal.

OSTN enhances CNP-dependent nuclear export of YAP1/WWTR1

We tried to delineate the linkage between OSTN-mediated signal and YAP1/WWTR1 using cultured osteoblasts. CNP regulates

Development (2017) 144, 334-344 doi:10.1242/dev.143354

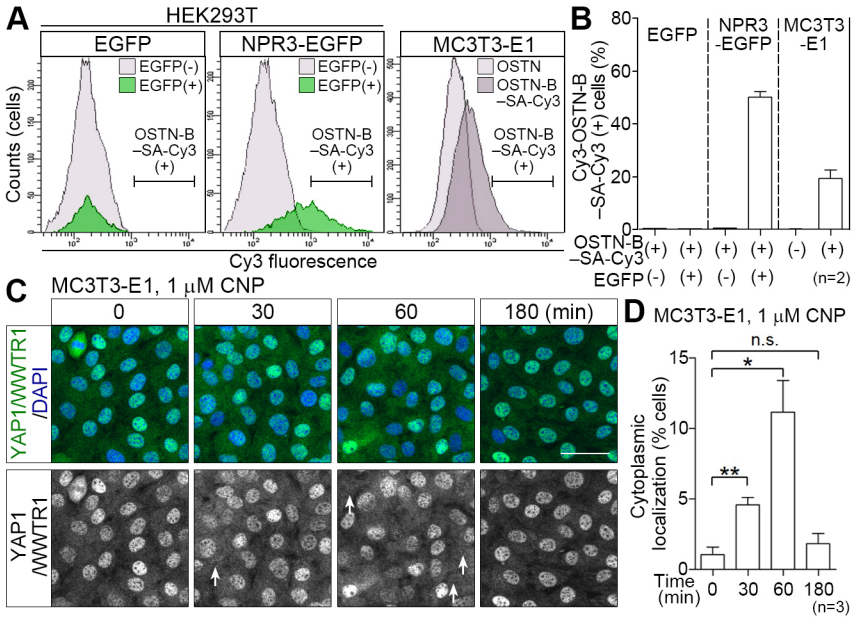

Fig. 6. CNP induces nuclear export of YAP1/WWTR1 in MC3T3-E1 cells. (A) Binding of biotin-labeled rat OSTN (OSTN-B) to EGFP (left) or NPR3-EGFP (center) overexpressed in HEK293T cells and that of unlabeled rat OSTN and OSTN-B to MC3T3-E1 cells (right) was analyzed by flow cytometry. Binding of OSTN-B was detected by Cy3-conjugated streptavidin (SA-Cy3). Note that OSTN-B binds to NPR3-EGFP and to endogenous receptors for OSTN expressed in MC3T3-E1 cells. (B) Quantitative analyses of A. (C) Representative images of anti-YAP1/WWTR1 immunostaining and DAPI staining of MC3T3-E1 cells stimulated with 1 μM CNP for the indicated time. Double staining with DAPI (blue) and YAP1/ WWTR1 (green) (top) and YAP1/WWTR1 staining alone (bottom) are shown. Arrows indicate cells exhibiting nuclear export of YAP1/WWTR1. (D) Quantitative analyses of nuclear export of YAP1/WWTR1 in C using three sets of cells. In each set, more than 100 cells were analyzed for immunoreactivity of YAP1/WWTR1. *P<0.05, **P<0.01; n.s., no significant difference between two groups. Error bars indicate s.e.m. Scale bar: 50 μm.

osteoblast differentiation through NPR2 (Suda et al., 1996). We assumed that OSTN might modify CNP-dependent signaling in osteoblasts, as OSTN is reported to bind to NPR3 to block binding of NPs to NPR3 (Moffatt et al., 2007). We first confirmed that OSTN binds to C-terminally EGFP-tagged NPR3 (NPR3-EGFP) in cultured cells using flow cytometry. HEK293T cells expressing NPR3-EGFP were bound to biotin-labeled rat (*Rattus norvegicus*) OSTN, which was detected by Cy3-conjugated streptavidin (Fig. 6A,B, Fig. S9A,C). Osteoblastic MC3T3-E1 cells also bound to OSTN (Fig. 6A,B). The binding of OSTN to NPR3-EGFP was competitive with CNP (Fig. S9B,C).

We further examined how CNP and OSTN affect the localization of YAP1 and WWTR1 in MC3T3-E1 cells. CNP induced nuclear export of YAP1/WWTR1 in a time-dependent (Fig. 6C,D) and dose-dependent (Fig. 7A,B) manner. This dose-dependent nuclear export paralleled an increase in cGMP (Fig. 7C) and reached a plateau when the cells were stimulated with 1 μM CNP. Even when induced with this saturated dose of CNP (1 μM), the nuclear export of YAP1/WWTR1 was enhanced by OSTN, whereas 1 μM OSTN alone did not induce nuclear export (Fig. 7D,E). CNP- and CNP/OSTN-dependent nuclear export of YAP1/WWTR1 was completely inhibited by the protein kinase G (PKG) inhibitor KT5823 (Fig. 7D,E), suggesting that cGMP-PKG signaling, presumably through CNP-activated NPR2, is essential for determining the localization of YAP1/WWTR1.

The consequence of nuclear export of YAP1/WWTR1 was reflected in the reduction of *Ctgf* mRNA expression when the cells were stimulated with CNP. A greater reduction in *Ctgf* mRNA was observed in cells stimulated with both 1 μM CNP and 1 μM OSTN, but not in those pretreated with KT5823 (Fig. 7F). Notably, MC3T3-E1 cells treated with 1 μM CNP still bound to 0.1 μM OSTN (Fig. 7G,H). The amount of biotin-labeled rat OSTN (0.1 μM) that bound to NPR3 was decreased by either unlabeled rat OSTN or CNP (Fig. S9A-C). Cy3-conjugated streptavidin was detected in MC3T3-E1 cells that were neither treated with unlabeled rat OSTN nor with biotin alone. Biotin-labeled rat OSTN (0.1 μM) binding to MC3T3-E1 cells was not affected by insulin, which was used as a negative control (Fig. S10A,B). Collectively, these data suggest that OSTN can bind to unidentified receptors besides NPR3 in MC3T3-E1 cells.

Because we found that endochondral bone formation was regulated by Ostn in zebrafish (Fig. 4), we examined the effect of Ostn on CNP-dependent localization of YAP1/WWTR1 in mouse chondrogenic ATDC5 cells. CNP induced nuclear export of YAP1/WWTR1 in both a time- and dose-dependent manner in ATDC5 cells, similar to MC3T3-E1 cells (Fig. S11A-D). These data indicate that a CNP-dependent signal induces the nuclear export of YAP1/WWTR1 in chondrogenic cells.

Enhancement of CNP-regulated nuclear export of YAP1/WWTR1 by OSTN depends on an NPR2-PKG signaling axis

We then examined whether CNP-induced nuclear export of YAP1/WWTR1 depends on NPR2. qRT-PCR analyses of *Npr2* mRNA in MC3T3-E1 cells treated with siRNA revealed the effective knockdown of *Npr2* (Fig. 8A, Fig. S12A). Furthermore, CNP-induced cGMP production, presumably through NPR2, was abolished in *Npr2* knockdown cells (Fig. 8B, Fig. S12B). Thus, we tested the effect of a reduction of *Npr2* on CNP-dependent nuclear export of YAP1/WWTR1 in the cells treated with these siRNAs. Nuclear export of YAP1/WWTR1 was reduced in the *Npr2* knockdown cells (Fig. 8C,D, Fig. S12C,D). Collectively, in osteoblasts, activation of NPR2 by CNP followed by PKG activation results in nuclear export of YAP1/WWTR1.

An increase in Yap1/Wwtr1-dependent transcription, as revealed by the EGFP reporter, in the ps of *ostn* morphants reflected the nuclear localization of Yap1/Wwtr1 (Fig. 5C), suggesting that a similar Npr2-mediated signal is activated in ps formation. The ps was shortened when Yap1/Wwtr1 were localized in nuclei, suggesting that activation of Yap1/Wwtr1 transcription results in shortening of the ps. To test whether an Npr2-dependent signal participates in ps formation, we examined how the reduction of Npr2 expression affects ps formation. Beforehand, we analyzed the expression of *npr2*, *npr3* and *nppcl* (*wu:fj39g12*) mRNAs. WISH analyses revealed that *npr2* mRNA is detected in head mesenchyme, pectoral fin bud/pectoral fin, ceratohyal and hyosymplectic. *npr3* mRNA was detected in the midbrain-hindbrain boundary and floor plate. *nppcl* mRNA was also detected in the brain (Fig. S13A-C). The *npr2* and *npr3* mRNAs were barely detected in the ps of larvae at 5 dpf (Fig. S13D). These

Development (2017) 144, 334-344 doi:10.1242/dev.143354

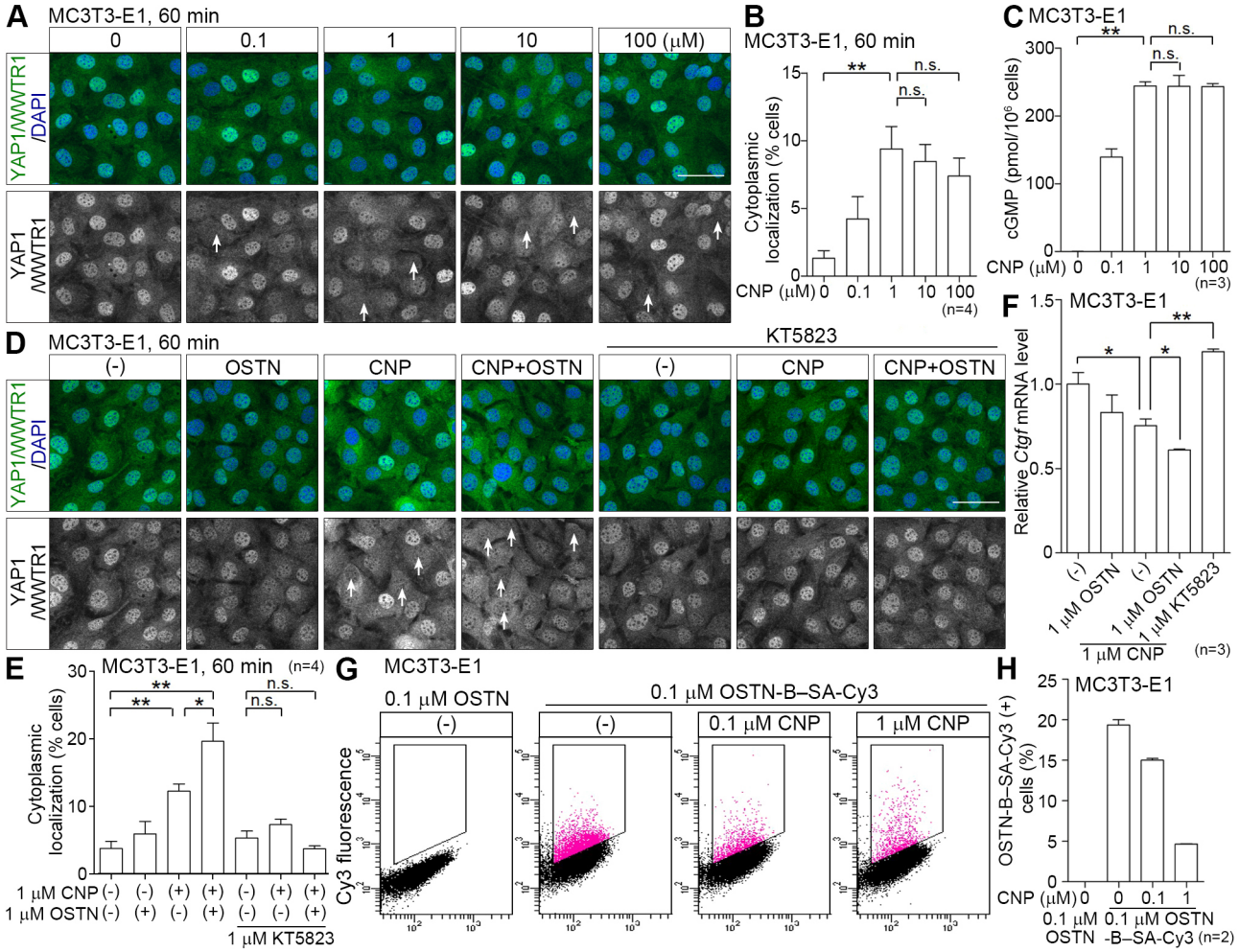

Fig. 7. OSTN enhances CNP-induced nuclear export of YAP1/WWTR1 in MC3T3-E1 cells. (A) Representative images of anti-YAP1/WWTR1 immunostaining and DAPI staining of MC3T3-E1 cells stimulated for 60 min with CNP at the doses indicated. (B) Quantitative analyses of nuclear export of YAP1/WWTR1 in A using four sets of cells. In each set, more than 100 cells were analyzed for immunoreactivity of YAP1/WWTR1. (C) Measurement of cGMP in MC3T3-E1 cells stimulated with CNP at the doses indicated for 15 min. (D) Representative images of anti-YAP1/WWTR1 immunostaining and DAPI staining of MC3T3-E1 cells pretreated with or without the PKG inhibitor KT5823 (1 μM) and stimulated for 60 min with CNP (1 μM) and Ostn (1 μM) as indicated on the top. Arrows indicate cells exhibiting cytoplasmic localization of YAP1/WWTR1. (E) The nuclear export of YAP1/WWTR1 in cells under the condition described in D were analyzed similar to B. (F) *Ctgf* mRNA expression analyzed by qRT-PCR using mRNAs obtained from MC3T3-E1 cells stimulated with the peptides and treated with KT5823 as indicated for 120 min. (G) Competitive binding of OSTN with CNP to MC3T3-E1 cells was analyzed by flow cytometry. The binding of OSTN-B in the presence of CNP to MC3T3-E1 cells is shown in the form of dot plot data. (H) Quantitative analyses of G. **P*<0.05, ***P*<0.01; n.s., no significant difference between two groups. Error bars indicate s.e.m. Scale bars: 50 μm.

data suggest that at least Nppcl-Npr2/Npr3 might function in zebrafish, although we failed to detect their expression in the ps.

The MOs against *npr2* were validated by examining splicing efficiency (Fig. S14A). *npr2* morphants exhibited a shortened ps at 5 dpf (Fig. 8E,F). Furthermore, this shortening of the ps was rescued by the injection of *npr2* mRNA into the larvae at 7 dpf (Fig. S14B,C). These data indicate that an Npr2-mediated signal is involved in the regulation of bone growth *in vivo*.

DISCUSSION

We identified Ostn as an endocrine hormone produced in the heart that regulates osteogenesis and chondrogenesis in zebrafish. Besides ANP and BNP, no endocrine hormones affecting remote organs have been reported for the heart. Although OSTN is proposed to belong to the NP family, it lacks the cysteine residues that render itself circular via a disulfide bridge that is conserved among the NP family members ANP, BNP and CNP (Potter et al., 2006; Riley and Smart, 2011). In addition, OSTN binds to NPR3 but not NPR2, thereby augmenting CNP-dependent NPR2 activation by inhibiting clearance of CNP in chondrocytes but not in osteoblasts (Moffatt et al., 2007). In agreement with this notion, our data suggest that Ostn contributes to both membranous bone formation and endochondral bone formation by inducing nuclear export of Yap1/Wwtr1. The present data also suggest that Ostn activates an unidentified receptor to regulate osteogenesis in zebrafish. Therefore, we provide evidence that the heart secretes a novel peptide regulating bone formation, although it is unlikely to belong to the NP family.

We found that membranous bones and endochondral bones were shortened in *ostn*^{ncv105} mutant larvae. At the early stage, Ostn specifically affected the growth of the ps among the cranial bones that develop according to intramembranous ossification. The ps develops earlier than other bones (Verreijdt et al., 2006) and so we could detect its shortening at an early stage (7 dpf). At the later stage, the other membranous bones were also shortened. Furthermore, cartilages were

Development (2017) 144, 334-344 doi:10.1242/dev.143354

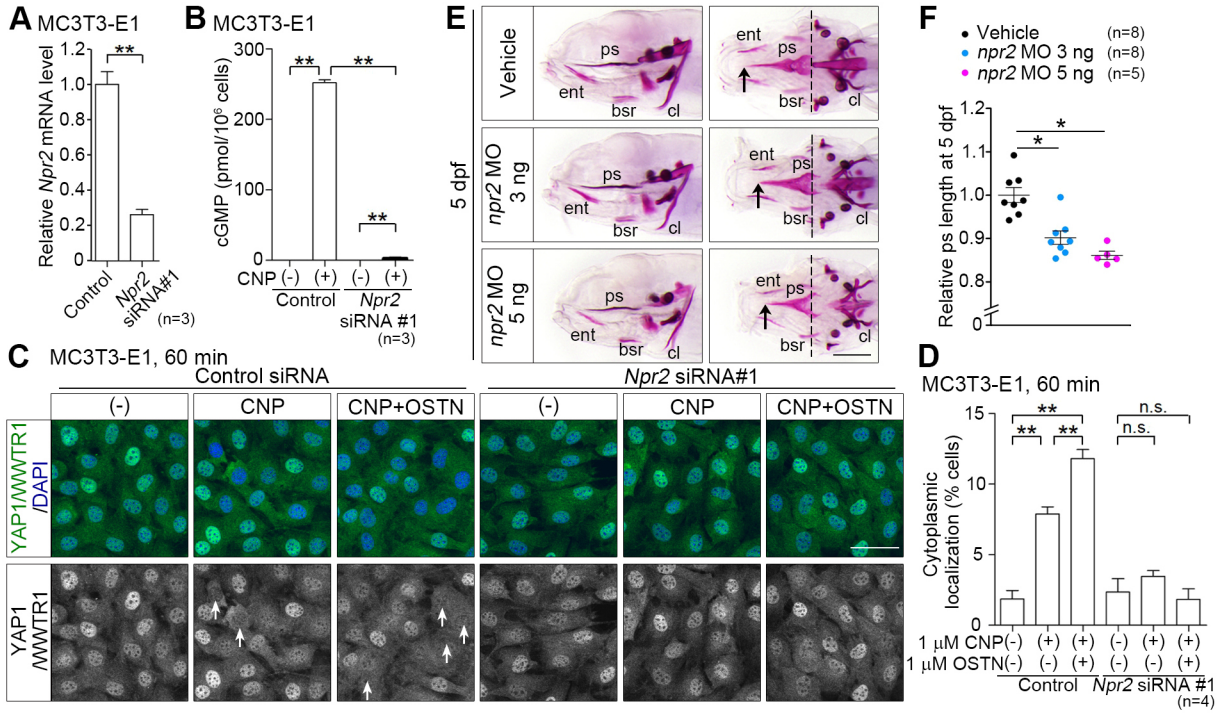

Fig. 8. CNP-induced nuclear export of YAP1/WWTR1 depends on NPR2. (A) qRT-PCR analyses validate the knockdown efficiency of siRNAs directed against *Npr2* mRNAs. MC3T3-E1 cells were treated with *Npr2* siRNA for 72 h. (B) cGMP levels in MC3T3-E1 cells pretreated with siRNAs for 72 h and stimulated with 1 μM CNP for 15 min as indicated. (C) Representative images of anti-YAP1/WWTR1 immunostaining and DAPI staining of MC3T3-E1 cells pretreated with either control siRNA or *Npr2* siRNA#1 and simulated with peptide (1 μM CNP and/or 1 μM OSTN) as indicated. Arrows indicate cells exhibiting nuclear export of YAP1 and WWTR1. (D) The nuclear export of YAP1/WWTR1 in the cells in C was analyzed similar to in Fig. 6D. (E) Representative images of Alizarin Red staining of 5 dpf larvae injected with vehicle, 3 ng or 5 ng *npr2* MO. Arrows and dashed lines indicate the tip and top of concave of the caudal end of the ps, respectively. (F) The length of ps in E was measured similar to in Fig. 3E. **P*<0.05, ***P*<0.01; n.s., no significant difference between two groups. Error bars indicate s.e.m. Scale bars: 50 μm in C; 200 μm in E.

shortened. These data suggest that a common signaling pathway regulates the growth of both bone types. Mammalian chondrocytes express *Runx2* and *Col10a1*, and zebrafish osteoblasts express these genes (Li et al., 2009). We noted no alteration of *runx2* expression in *ostn*^{ncv105} larvae. Therefore, an Ostn-mediated signal might be involved in promoting the expression of genes essential for bone matrix apposition.

OSTN augments the CNP-dependent nuclear export of YAP1/WWTR1 in osteoblasts and chondrocytes. It is of note that CNP induces the export of YAP1/WWTR1 in these cells. There have been no reports that NPs regulate the localization of YAP1/WWTR1. Inhibition of PKG inhibited the export of YAP1/WWTR1. Although protein kinase A, another Ser/Thr kinase, is reported to determine the localization of YAP1 through LATS kinase (Iglesias-Bartolome et al., 2015; Kim et al., 2013), PKG-dependent regulation has not been reported. *Ostn* Tg mice exhibit elongated bones and kyphosis, which are also found in *Bnp* Tg, *Cnp* Tg and *Npr3* knockout mice (Jaubert et al., 1999; Kake et al., 2009; Matsukawa et al., 1999; Yasoda et al., 2004). Elongation of bones is ascribed to modulation of CNP-NPR3 signaling by OSTN in chondrocytes (Moffatt et al., 2007). OSTN binds to NPR3 and is proposed to inhibit clearance of CNP, resulting in augmentation of a CNP-dependent signal. Notably, OSTN augmented YAP1/WWTR1 nuclear export at a saturating concentration of CNP for NP receptors. These results suggested that OSTN binds to an unidentified receptor to modulate CNP-dependent signaling downstream of NPR2, as OSTN itself did not induce nuclear export of YAP1/WWTR1 in osteoblasts. We need to identify the OSTN-specific receptor in order to clearly delineate the OSTN signaling that is not through NPR3.

The role for a YAP1/WWTR1-dependent signal in osteogenesis remains controversial. WWTR1 regulates the differentiation of MSCs to osteoblasts (Hong et al., 2005). On the one hand, overexpression of WWTR1 in mice leads to an increased bone mass via RUNX2-dependent transcription (Yang et al., 2013). On the other hand, YAP1 binds to RUNX2 to represses its transcriptional activity (Zaidi et al., 2004). One group reports that fibroblast growth factor 2 (FGF2) downregulates WWTR1 in MC3T3-E1 cells to induce their proliferation (Eda et al., 2008), whereas another group demonstrated that FGF2 induces the differentiation of osteoblasts (Byun et al., 2014). Therefore, it is still controversial how YAP1/WWTR1 function in osteoblasts after their differentiation from MSCs *in vivo*. Proliferation, differentiation and apoptosis of osteoblasts are not altered in *ostn* morphants. However, chondrocytes were smaller in *ostn* mutants than in the control, suggesting that a Yap1/Wwtr1-mediated signal might participate in bone matrix deposition or mineralization. Expression of *col10a1* mRNA was decreased in *ostn*^{ncv105} larvae at 7 dpf. Because mRNAs were prepared from whole larvae, it is unclear whether this decrease was attributable to that in osteoblasts or chondrocytes. Expression of Col10a1 has been reported to be transcriptionally inhibited by Yap1 (Deng et al., 2016), and our results are consistent with this.

CTGF-dependent bone formation appears to be complicated. While *Ctgf*-deficient mice show impaired chondrocyte proliferation and matrix composition in the hypertrophic chondrocytes (Ivkovic et al., 2003), overexpression of CTGF from the osteocalcin promoter results in impairment of osteoblast activity due to decreased mineral apposition (Smerdel-Ramoya et al., 2008). However, another study reports that CTGF-deficient osteoblasts

Development (2017) 144, 334-344 doi:10.1242/dev.143354

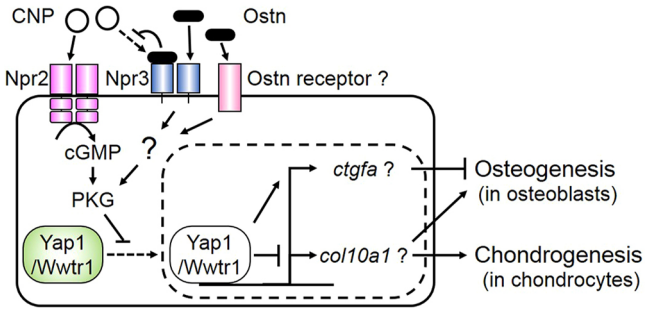

Fig. 9. Model for how Ostn regulates bone formation. (A) In zebrafish osteoblasts and chondrocytes, CNP induces nuclear export of Yap1/Wwtr1 through Npr2-cGMP-PKG signaling. Because Yap1 is known to inhibit the transcription of *col10a1*, Ostn might induce nuclear export of Yap1 and the subsequent expression of Col10a1 in osteoblasts and chondrocytes and subsequent repression of Ctgfa in osteoblasts. Collectively, Ostn secreted from the heart and other tissues binds to Npr3 and the unidentified Ostn receptor to enhance the CNP-induced nuclear export of Yap1/Wwtr1 and promote osteogenesis and chondrogenesis.

exhibit reduced proliferation but normal mineralization (Mundy et al., 2014). These results suggest that CTGF expression promoted by YAP1/WWTR1 might function in bone formation in a stage-dependent and cell-dependent manner.

Ostn from the CS, which controls calcium homeostasis, might also contribute to bone formation. We found that Ostn is expressed in the CS where Casr and stanniocalcin are expressed (Lin et al., 2014; Tseng et al., 2009). In the CS, Casr senses the extracellular Ca^{2+} and regulates stanniocalcin, which acts on Na^{+}/K^{+}-ATPase-rich cells in zebrafish that function in Ca^{2+} absorption (Tseng et al., 2009). Therefore, if Ostn regulates Ca^{2+} balance through the CS, the impaired bone formation found in *ostn*^{ncv105} larvae might be ascribed to dysfunction of the CS.

In summary, we demonstrate that Ostn produced in CMs contributes to the formation of both membranous and endochondral bone (Fig. 9). OSTN enhanced peak CNP-dependent nuclear export of YAP1/WWTR1 in osteoblasts and chondrocytes. Our data suggest that Ostn regulates osteogenesis and chondrogenesis in zebrafish cooperatively through NP-dependent signaling and through an unidentified Ostn receptor-mediated signaling.

MATERIALS AND METHODS

Zebrafish husbandry

Zebrafish were maintained under standard conditions (Westerfield, 2007). Experiments using zebrafish were approved by the Institutional Animal Committee of the National Cerebral and Cardiovascular Center and performed according to the guidelines of the institute. Embryos and larvae were staged by hpf at 28°C (Kimmel et al., 1995).

Plasmids

Construction of Tol2-based plasmids used to establish Tg zebrafish lines is described in the supplementary Materials and Methods. Primers for cloning are listed in Table S1.

Tg and mutant fish lines

Transgenic zebrafish lines and the *ostn*^{ncv105} mutant line were established as described in the supplementary Materials and Methods. The *Tg(UAS:EGFP)* fish line was provided by K. Kawakami (National Institute of Genetics, Japan; Asakawa et al., 2008). Primers for genotyping are listed in Table S1.

FACS and RNA-seq

mCherry-positive or tdEos-positive cells were isolated by FACS (see the supplementary Materials and Methods) from *Tg(myl7:NLS-mCherry)* or *Tg(myl7:actn2-tdEos)* larvae, respectively. The isolated cells were subjected to RNA-seq analyses as described in the supplementary Materials and Methods.

RT-PCR

Total RNA was isolated from zebrafish larvae, mouse organs or mouse MC3T3-E1 cells for RT-PCR of cDNA as described in the supplementary Materials and Methods. RT-PCR primers are listed in Table S1.

WISH

Zebrafish embryos and larvae at 1-4 dpf were hybridized with digoxigenin-labeled antisense RNA probes as described in the supplementary Materials and Methods.

Bone staining

Zebrafish larvae at 5-10 dpf were stained for membranous bones with Alizarin Red S and for cartilage with Alcian Blue 8GX as described in the supplementary Materials and Methods.

Microinjection of MOs and mRNA

For gene knockdown, one-cell stage zebrafish embryos were injected with *ostn*, *npr2*, *ctgfa* or control MOs. For protein overexpression, mRNA was injected into one-cell stage zebrafish embryos. For details see the supplementary Materials and Methods.

Cell culture and siRNA-mediated knockdown

Mouse MC3T3-E1, ATDC5 and human HEK293T cells were cultured, and transfections with plasmids or siRNAs (Table S2) were performed, as described in the supplementary Materials and Methods.

Microscopy, image processing and movies

Larvae were anesthetized and mounted in 1% low-melting agarose on a 35 mm diameter glass-base dish (Asahi Techno Glass) as previously described (Kashiwada et al., 2015). Fluorescence images were recorded with a FV1000 or FV1200 confocal microscope with 20× water objective lens (XLUMPlanFL, 1.0 NA) or a FV1000PME multi-photon microscope with 25× water objective lens (XLPlan, 1.05 NA) (all Olympus). Images were processed with FV10-ASW 4.1 software (Olympus) and analyzed using Imaris 7.7.1 software (Bitplane). Head length was measured using a stereo microscope as described in the supplementary Materials and Methods. Larval heart beat was recorded by lightsheet microscopy or in brightfield movies as described in the supplementary Materials and Methods.

OSTN binding assay

Streptavidin-conjugated Cy3 was incubated with biotin-labeled rat OSTN to form OSTN-B–SA-Cy3. HEK293T cells expressing NPR3-EGFP or EGFP and MC3T3-E1 cells were suspended, incubated with OSTN-B–SA-Cy3, and fluorescence intensities measured by FACS as described in the supplementary Materials and Methods.

Apoptosis and cell proliferation assays

Apoptotic cells in 6 dpf zebrafish larvae were assessed by TUNEL assay, and the proliferation of cells in 5 dpf zebrafish larvae was analyzed by EdU incorporation, as described in the supplementary Materials and Methods.

cGMP

cGMP was measured in MC3T3-E1 cells stimulated with CNP as described in the supplementary Materials and Methods.

Immunocytochemical analyses

MC3T3-E1 and ATDC5 cells were subjected to immunocytochemistry with anti-YAP1/WWTR1 antibody (Santa Cruz, sc-101199) at 1:300 as described in the supplementary Materials and Methods.

Development (2017) 144, 334-344 doi:10.1242/dev.143354

Quantitative analyses of fluorescence

To quantify Yap1/Wwtr1 transcriptional activity in zebrafish membranous bone, confocal stack fluorescence images of EGFP and Alizarin Red in the membranous bone regions of *Tg(Ola.sp7:Gal4db-Hsa.TEAD2ΔN-2A-mCherry);(UAS:EGFP)* 6 dpf larvae were recorded. The mean EGFP fluorescence intensity within a 100 μm^2 circle of EGFP-positive cells was measured using the FV10-ASW 4.1 software.

To quantify the percentage of MC3T3-E1 and ATDC5 cells showing YAP1/WWTR1 cytoplasmic localization, the mean fluorescence intensity of YAP1/WWTR1 staining inside a circle (8 μm in diameter) in the cytoplasm or nucleus was measured for each cell using MetaMorph software (Molecular Devices). Cells with a ratio of cytoplasmic to nuclear intensity of greater than one were considered to be positive for the cytoplasmic localization of YAP1/WWTR1. The percentage of cells showing cytoplasmic localization among total cells was calculated using unbiased images of four different microscopy fields.

Statistical analysis

Data are represented as mean±s.e.m. Statistical significance was determined by Student's *t*-test for paired samples or by one-way analysis of variance (ANOVA) with Turkey's test. $P<0.05$ was considered statistically significant.

Acknowledgements

We thank Koichi Kawakami (National Institute of Genetics, Japan) for providing *Tg(UAS:EGFP)* fish; Gary Felsenfeld (National Institutes of Health, USA), Hiroshi Nishina (Tokyo Medical and Dental University, Japan) and John Kuwada (University of Michigan, USA) for valuable materials; Manami Sone, Keiko Hiratomi, Wakana Koeda, Mayumi Ueda and Tomo Babazono for excellent technical assistance; and Eri Okamoto and Shigemi Toyoshima for fish care. We are grateful to the National BioResource Project from MEXT, Japan for several fish lines.

Competing interests

The authors declare no competing or financial interests.

Author contributions

Conceptualization: H.W.-T., S.F., N.M.; Formal analysis and investigation: A.C., H.W.-T., M.U., K.T., T.M., H.F., H.H., M.H.; Writing – original draft preparation: A.C., H.W.-T.; Writing – review and editing: N.M.

Funding

This work was partly supported by Japan Society for the Promotion of Science KAKENHI grants (22122003 and 16H02618), Japan Agency for Medical Research and Development AMED-CREST grant (13414779 to N.M.), by Health and Labour Sciences Research Grant to N.M., and by a grant from Takeda Science Foundation to N.M.

Data availability

RNA-seq data are available at ArrayExpress (EMBL-EBI) under accession number E-MTAB-5323.

Supplementary information

Supplementary information available online at
http://dev.biologists.org/lookup/doi/10.1242/dev.143354.supplemental

References

Arita, Y., Nakaoka, Y., Matsunaga, T., Kidoya, H., Yamamizu, K., Arima, Y., Kataoka-Hashimoto, T., Ikeoka, K., Yasui, T., Masaki, T. et al. (2014). Myocardium-derived angiopoietin-1 is essential for coronary vein formation in the developing heart. *Nat. Commun.* **5**, 4552.

Asakawa, K., Suster, M. L., Mizusawa, K., Nagayoshi, S., Kotani, T., Urasaki, A., Kishimoto, Y., Hibi, M. and Kawakami, K. (2008). Genetic dissection of neural circuits by Tol2 transposon-mediated Gal4 gene and enhancer trapping in zebrafish. *Proc. Natl. Acad. Sci. USA* **105**, 1255-1260.

Becker, J. R., Chatterjee, S., Robinson, T. Y., Bennett, J. S., Panakova, D., Galindo, C. L., Zhong, L., Shin, J. T., Coy, S. M., Kelly, A. E. et al. (2014). Differential activation of natriuretic peptide receptors modulates cardiomyocyte proliferation during development. *Development* **141**, 335-345.

Byun, M. R., Kim, A. R., Hwang, J.-H., Kim, K. M., Hwang, E. S. and Hong, J.-H. (2014). FGF2 stimulates osteogenic differentiation through ERK induced TAZ expression. *Bone* **58**, 72-80.

Dauphinee, S. M., Eva, M. M., Yuki, K. E., Herman, M., Vidal, S. M. and Malo, D. (2013). Characterization of two ENU-induced mutations affecting mouse skeletal morphology. *G3 (Bethesda)* **3**, 1753-1758.

Deng, Y., Wu, A., Li, P., Li, G., Qin, L., Song, H. and Mak, K. K. (2016). Yap1 regulates multiple steps of chondrocyte differentiation during skeletal development and bone repair. *Cell Rep.* **14**, 2224-2237.

Eda, H., Aoki, K., Marumo, K., Fujii, K. and Ohkawa, K. (2008). FGF-2 signaling induces downregulation of TAZ protein in osteoblastic MC3T3-E1 cells. *Biochem. Biophys. Res. Commun.* **366**, 471-475.

Hagiwara, H., Sakaguchi, H., Itakura, M., Yoshimoto, T., Furuya, M., Tanaka, S. and Hirose, S. (1994). Autocrine regulation of rat chondrocyte proliferation by natriuretic peptide C and its receptor, natriuretic peptide receptor-B. *J. Biol. Chem.* **269**, 10729-10733.

Hong, J.-H., Hwang, E. S., McManus, M. T., Amsterdam, A., Tian, Y., Kalmukova, R., Mueller, E., Benjamin, T., Spiegelman, B. M., Sharp, P. A. et al. (2005). TAZ, a transcriptional modulator of mesenchymal stem cell differentiation. *Science* **309**, 1074-1078.

Iglesias-Bartolome, R., Torres, D., Marone, R., Feng, X., Martin, D., Simaan, M., Chen, M., Weinstein, L. S., Taylor, S. S., Molinolo, A. A. et al. (2015). Inactivation of a Galpha(s)-PKA tumour suppressor pathway in skin stem cells initiates basal-cell carcinogenesis. *Nat. Cell Biol.* **17**, 793-803.

Ivkovic, S., Yoon, B. S., Popoff, S. N., Safadi, F. F., Libuda, D. E., Stephenson, R. C., Daluiski, A. and Lyons, K. M. (2003). Connective tissue growth factor coordinates chondrogenesis and angiogenesis during skeletal development. *Development* **130**, 2779-2791.

Jaubert, J., Jaubert, F., Martin, N., Washburn, L. L., Lee, B. K., Eicher, E. M. and Guenet, J.-L. (1999). Three new allelic mouse mutations that cause skeletal overgrowth involve the natriuretic peptide receptor C gene (Npr3). *Proc. Natl. Acad. Sci. USA* **96**, 10278-10283.

Kake, T., Kitamura, H., Adachi, Y., Yoshioka, T., Watanabe, T., Matsushita, H., Fujii, T., Kondo, E., Tachibe, T., Kawase, Y. et al. (2009). Chronically elevated plasma C-type natriuretic peptide level stimulates skeletal growth in transgenic mice. *Am. J. Physiol. Endocrinol. Metab.* **297**, E1339-E1348.

Karsenty, G., Kronenberg, H. M. and Settembre, C. (2009). Genetic control of bone formation. *Annu. Rev. Cell Dev. Biol.* **25**, 629-648.

Kashiwada, T., Fukuhara, S., Terai, K., Tanaka, T., Wakayama, Y., Ando, K., Nakajima, H., Fukui, H., Yuge, S., Saito, Y. et al. (2015). beta-Catenin-dependent transcription is central to Bmp-mediated formation of venous vessels. *Development* **142**, 497-509.

Kim, M., Kim, M., Lee, S., Kuninaka, S., Saya, H., Lee, H., Lee, S. and Lim, D.-S. (2013). cAMP/PKA signalling reinforces the LATS-YAP pathway to fully suppress YAP in response to actin cytoskeletal changes. *EMBO J.* **32**, 1543-1555.

Kimmel, C. B., Ballard, W. W., Kimmel, S. R., Ullmann, B. and Schilling, T. F. (1995). Stages of embryonic development of the zebrafish. *Dev. Dyn.* **203**, 253-310.

Knopf, F., Hammond, C., Chekuru, A., Kurth, T., Hans, S., Weber, C. W., Mahatma, G., Fisher, S., Brand, M., Schulte-Merker, S. et al. (2011). Bone regenerates via dedifferentiation of osteoblasts in the zebrafish fin. *Dev. Cell* **20**, 713-724.

Komatsu, Y., Chusho, H., Tamura, N., Yasoda, A., Miyazawa, T., Suda, M., Miura, M., Ogawa, Y. and Nakao, K. (2002). Significance of C-type natriuretic peptide (CNP) in endochondral ossification: analysis of CNP knockout mice. *J. Bone Miner. Metab.* **20**, 331-336.

Komori, T., Yagi, H., Nomura, S., Yamaguchi, A., Sasaki, K., Deguchi, K., Shimizu, Y., Bronson, R. T., Gao, Y.-H., Inada, M. et al. (1997). Targeted disruption of Cbfa1 results in a complete lack of bone formation owing to maturational arrest of osteoblasts. *Cell* **89**, 755-764.

Li, N., Felber, K., Elks, P., Croucher, P. and Roehl, H. H. (2009). Tracking gene expression during zebrafish osteoblast differentiation. *Dev. Dyn.* **238**, 459-466.

Lin, C.-H., Su, C.-H. and Hwang, P.-P. (2014). Calcium-sensing receptor mediates Ca(2+) homeostasis by modulating expression of PTH and stanniocalcin. *Endocrinology* **155**, 56-67.

Long, F. and Ornitz, D. M. (2013). Development of the endochondral skeleton. *Cold Spring Harb. Perspect. Biol.* **5**, a008334.

Matsukawa, N., Grzesik, W. J., Takahashi, N., Pandey, K. N., Pang, S., Yamauchi, M. and Smithies, O. (1999). The natriuretic peptide clearance receptor locally modulates the physiological effects of the natriuretic peptide system. *Proc. Natl. Acad. Sci. USA* **96**, 7403-7408.

Moffatt,P. and Thomas,G. P. (2009). Osteocrin–beyond just another bone protein? *Cell Mol. Life Sci.* **66**, 1135-1139.

Moffatt, P., Thomas, G., Sellin, K., Bessette, M.-C., Lafreniere, F., Akhouayri, O., St-Arnaud, R. and Lanctot, C. (2007). Osteocrin is a specific ligand of the natriuretic Peptide clearance receptor that modulates bone growth. *J. Biol. Chem.* **282**, 36454-36462.

Mundy, C., Gannon, M. and Popoff, S. N. (2014). Connective tissue growth factor (CTGF/CCN2) negatively regulates BMP-2 induced osteoblast differentiation and signaling. *J. Cell Physiol.* **229**, 672-681.

Nishizawa, H., Matsuda, M., Yamada, Y., Kawai, K., Suzuki, E., Makishima, M., Kitamura, T. and Shimomura, I. (2004). Musclin, a novel skeletal muscle-derived secretory factor. *J. Biol. Chem.* **279**, 19391-19395.

Ogawa, T. and de Bold, A. J. (2014). The heart as an endocrine organ. *Endocr. Connect.* **3**, R31-R44.
Potter, L. R., Abbey-Hosch, S. and Dickey, D. M. (2006). Natriuretic peptides, their receptors, and cyclic guanosine monophosphate-dependent signaling functions. *Endocr. Rev.* **27**, 47-72.
Riley, P. R. and Smart, N. (2011). Vascularizing the heart. *Cardiovasc. Res.* **91**, 260-268.
Schilling, T. F. and Kimmel, C. B. (1997). Musculoskeletal patterning in the pharyngeal segments of the zebrafish embryo. *Development* **124**, 2945-2960.
Smerdel-Ramoya, A., Zanotti, S., Stadmeyer, L., Durant, D. and Canalis, E. (2008). Skeletal overexpression of connective tissue growth factor impairs bone formation and causes osteopenia. *Endocrinology* **149**, 4374-4381.
Soltanoff, C. S., Yang, S., Chen, W. and Li, Y.-P. (2009). Signaling networks that control the lineage commitment and differentiation of bone cells. *Crit. Rev. Eukaryot. Gene Expr.* **19**, 1-46.
Spoorendonk, K. M., Peterson-Maduro, J., Renn, J., Trowe, T., Kranenbarg, S., Winkler, C. and Schulte-Merker, S. (2008). Retinoic acid and Cyp26b1 are critical regulators of osteogenesis in the axial skeleton. *Development* **135**, 3765-3774.
Stepan, H., Leitner, E., Siems, W.-E., Maul, B. and Walther, T. (1999). mRNA quantification of C-type natriuretic peptide in brain areas of rodents. *Peptides* **20**, 1243-1245.
Stepan, H., Faber, R., Stegemann, S., Schultheiss, H.-P. and Walther, T. (2002). Expression of C-type natriuretic peptide in human placenta and myometrium in normal pregnancies and pregnancies complicated by intrauterine growth retardation. Preliminary results. *Fetal Diagn. Ther.* **17**, 37-41.
Subbotina, E., Sierra, A., Zhu, Z., Gao, Z., Koganti, S. R. K., Reyes, S., Stepniak, E., Walsh, S. A., Acevedo, M. R., Perez-Terzic, C. M. et al. (2015). Musclin is an activity-stimulated myokine that enhances physical endurance. *Proc. Natl. Acad. Sci. USA* **112**, 16042-16047.
Suda, M., Tanaka, K., Fukushima, M., Natsui, K., Yasoda, A., Komatsu, Y., Ogawa, Y., Itoh, H. and Nakao, K. (1996). C-type natriuretic peptide as an autocrine/paracrine regulator of osteoblast. Evidence for possible presence of bone natriuretic peptide system. *Biochem. Biophys. Res. Commun.* **223**, 1-6.
Suda, M., Ogawa, Y., Tanaka, K., Tamura, N., Yasoda, A., Takigawa, T., Uehira, M., Nishimoto, H., Itoh, H., Saito, Y. et al. (1998). Skeletal overgrowth in transgenic mice that overexpress brain natriuretic peptide. *Proc. Natl. Acad. Sci. USA* **95**, 2337-2342.
Tamura, N., Doolittle, L. K., Hammer, R. E., Shelton, J. M., Richardson, J. A. and Garbers, D. L. (2004). Critical roles of the guanylyl cyclase B receptor in endochondral ossification and development of female reproductive organs. *Proc. Natl. Acad. Sci. USA* **101**, 17300-17305.
Thomas, G., Moffatt, P., Salois, P., Gaumond, M.-H., Gingras, R., Godin, E., Miao, D., Goltzman, D. and Lanctot, C. (2003). Osteocrin, a novel bone-specific secreted protein that modulates the osteoblast phenotype. *J. Biol. Chem.* **278**, 50563-50571.
Tseng, D.-Y., Chou, M.-Y., Tseng, Y.-C., Hsiao, C.-D., Huang, C.-J., Kaneko, T. and Hwang, P.-P. (2009). Effects of stanniocalcin 1 on calcium uptake in zebrafish (Danio rerio) embryo. *Am. J. Physiol. Regul. Integr. Comp. Physiol.* **296**, R549-R557.
Varelas, X. (2014). The Hippo pathway effectors TAZ and YAP in development, homeostasis and disease. *Development* **141**, 1614-1626.
Verreijdt, L., Debiais-Thibaud, M., Borday-Birraux, V., Van der Heyden, C., Sire, J.-Y. and Huysseune, A. (2006). Expression of the dlx gene family during formation of the cranial bones in the zebrafish (Danio rerio): differential involvement in the visceral skeleton and braincase. *Dev. Dyn.* **235**, 1371-1389.
von, G. A., Lin, Z., Schlegelmilch, K., Honor, L. B., Pan, G. M., Buck, J. N., Ma, Q., Ishiwata, T., Zhou, B., Camargo, F. D. et al. (2012). YAP1, the nuclear target of Hippo signaling, stimulates heart growth through cardiomyocyte proliferation but not hypertrophy. *Proc. Natl. Acad. Sci. USA* **109**, 2394-2399.
Westerfield, M. (2007). *The Zebrafish Book. A Guide for the Laboratory Used of Zebrafsih (Danio rerio)*, 5th edn. Eugene, USA: University of Oregon Press.
Yang, J.-Y., Cho, S. W., An, J. H., Jung, J. Y., Kim, S. W., Kim, S. Y., Kim, J. E. and Shin, C. S. (2013). Osteoblast-targeted overexpression of TAZ increases bone mass in vivo. *PLoS ONE* **8**, e56585.
Yasoda, A., Komatsu, Y., Chusho, H., Miyazawa, T., Ozasa, A., Miura, M., Kurihara, T., Rogi, T., Tanaka, S., Suda, M. et al. (2004). Overexpression of CNP in chondrocytes rescues achondroplasia through a MAPK-dependent pathway. *Nat. Med.* **10**, 80-86.
Zaidi, S. K., Sullivan, A. J., Medina, R., Ito, Y., van Wijnen, A. J., Stein, J. L., Lian, J. B. and Stein, G. S. (2004). Tyrosine phosphorylation controls Runx2-mediated subnuclear targeting of YAP to repress transcription. *EMBO J.* **23**, 790-799.
Zhang, H., Liu, C.-Y., Zha, Z.-Y., Zhao, B., Yao, J., Zhao, S., Xiong, Y., Lei, Q.-Y. and Guan, K.-L. (2009). TEAD transcription factors mediate the function of TAZ in cell growth and epithelial-mesenchymal transition. *J. Biol. Chem.* **284**, 13355-13362.
Zhao, B., Wei, X., Li, W., Udan, R. S., Yang, Q., Kim, J., Xie, J., Ikenoue, T., Yu, J., Li, L. et al. (2007). Inactivation of YAP oncoprotein by the Hippo pathway is involved in cell contact inhibition and tissue growth control. *Genes Dev.* **21**, 2747-2761.
Zhao, B., Ye, X., Yu, J., Li, L., Li, W., Li, S., Yu, J., Lin, J. D., Wang, C.-Y., Chinnaiyan, A. M. et al. (2008). TEAD mediates YAP-dependent gene induction and growth control. *Genes Dev.* **22**, 1962-1971.
Zhao, B., Li, L., Lei, Q. and Guan, K. L. (2010). The Hippo-YAP pathway in organ size control and tumorigenesis: an updated version. *Genes Dev.* **24**, 862-874.
Zhou, X., Zhang, Z., Feng, J. Q., Dusevich, V. M., Sinha, K., Zhang, H., Darnay, B. G. and de Crombrugghe, B. (2010). Multiple functions of Osterix are required for bone growth and homeostasis in postnatal mice. *Proc. Natl. Acad. Sci. USA* **107**, 12919-12924.

Supplementary Materials and Methods

Plasmids

A promoter/enhancer sequence (chr1: 28,292,241 – 28,293,179) of zebrafish (*Danio rerio*) *crystallin, alpha A* (*cryaa)* gene (*cryaa* promoter), that (chr5:9,071,149-9,075,275) of medaka (*Oryzias latipes*) *Sp7 transcription factor* (*sp7*) gene (*Ola.sp7* promoter), and that (chr6:45,506,296-45,506,852) of human (*Homo sapiens*) *runt related transcription factor 2* (*RUNX2*) gene (*Hsa.RUNX2* promoter) were obtained by the PCR amplification of species-specific genomic DNA, respectively (Knopf et al., 2011; Kurita et al., 2003; Spoorendonk et al., 2008). The medaka genomic DNA was kindly provided by H. Nishina (Tokyo Medical and Dental University, Japan). A promoter/enhancer sequence of *myosin, light chain 7, regulatory* (*myl7*) gene (*myl7* promoter) was described previously (Fukui et al., 2014).

Either full length or partial cDNA fragments encoding zebrafish *actinin, alpha 2* (*actn2*), *osteocrin* (*ostn*), *calcium-sensing receptor* (*casr*), *myogenic differentiation 1* (*myod1*), *sex determining region Y-box 9a* (*sox9a*), *runx2b, secreted phosphoprotein 1* (*spp1*), *collagen, type X, alpha 1* (*col10a1*), *natriuretic peptide receptor 2* (*npr2*), *natriuretic peptide receptor 3* (*npr3*), *natriuretic peptide C, like* (*nppcl*), mouse (*Mus musculus*) Ostn (*Mmu.Ostn*), and human *NPR3* (*Hsa.NPR3*) were amplified by PCR using species-specific cDNA libraries as templates and cloned into pCR4 Blunt TOPO vector (Thermo Fisher scientific). Primers used for cloning were listed in supplementary data (Table S1). cDNA fragments of zebrafish *connective tissue growth factor a* (*ctgfa), yes-associated protein 1* (*yap1*)*-5SA*, Yap1–Tead interfering peptide (*ytip*), *runx2a, sp7* and *Hsa. TEA domain transcription factor 2 (TEAD2)* were described previously (Fukui et al., 2014; Kashiwada et al., 2015; Uemura et al., 2016). A cDNA fragment encoding a

yeast (*Saccharomyces cerevisiae*) GAL4-DNA-binding domain (*Gal4db*) fused to two transcriptional activation domains from VP16 (*GAL4FF*) was derived from a pCS2+Gal4FF vector.

To generate a pTol2-myl7 vector, a myl7 promoter was inserted into pTol2 vector, which was kindly provided by K. Kawakami (National Institute of Genetics, Japan) (Kawakami et al., 2004; Urasaki et al., 2006).

To construct a pTol2-myl7:actn2-tdEos plasmid, *EGFP* cDNA was removed from pEGFP-N1 vector (Clontech) and replaced with *tandem (td) Eos* cDNA derived from pcDNA3Flag-td-EosFP (Funakoshi) (ptdEos-N1 vector). A ptdEos-N1-actn2 plasmid was constructed by inserting *actn2* cDNA into the ptdEos-N1 vector. Finally, a cDNA fragment encoding *tdEos*-tagged *actn2* was subcloned into the pTol2-myl7 vector.

To construct a pTol2-myl7:ostn-HS4-hsp70l:EGFP plasmid, a chicken (*Gallus gallus*) *β-globin* insulator (*HS4*) derived from pJC13-1 vector, which was a gift from G. Felsenfeld (National Institute of Health, USA) (Chung et al., 1993) and a multiple cloning site (MCS) were sequentially subcloned into the pTol2-myl7: nuclear localization signal (NLS) tagged–monomeric (m) Cherry vector (Fukui et al., 2014) (pTol2-myl7:NLS-mCherry-HS4-MCS). A zebrafish heat shock protein (*hsp70l*) promoter followed by EGFP (hsp70l:EGFP) derived from pHSP70/4 EGFP plasmid (provided by J. Kuwada, University of Michigan, USA) (Halloran et al., 2000) were inserted into the pTol2-myl7:NLS-mCherry-HS4-MCS to generate pTol2-myl7:NLS-mCherry-HS4- hsp70l:EGFP. Finally, a *NLS-mCherry* cDNA fragment was removed and replaced with an *ostn* cDNA fragment.

To construct a pTol2-Ola.sp7:EGFP plasmid, a DNA fragment encoding *EGFP* and an Ola.sp7 promoter were sequentially inserted in to the pTol2 vector.

To construct a pTol2-Ola.sp7:GAL4FF-2A-mCherry plasmid, a cDNA fragment encoding *GAL4FF* followed by *2A* peptide and *mCherry* (GAL4FF-2A-mCherry) and an Ola.sp7 promoter were sequentially inserted into the pTol2 vector. To construct a pTol2-Hsa.RUNX2:GAL4FF-2A-mCherry plasmid, a cDNA fragment encoding *GAL4FF-2A-mCherry* and a Hsa.RUNX2 promoter followed by a TATA box region of an adenovirus E1b minimal promoter derived from pFR-Luc (Stratagene) were sequentially inserted into the pTol2 vector. To construct a pTol2-Ola.sp7:Gal4db-Hsa.TEADΔN-2A-mCherry plasmid, a cDNA fragment encoding *Gal4db* was fused to *Hsa.TEAD2* cDNA lacking amino-terminus (1-113 a.a.) followed by *2A* peptide and *mCherry* (Gal4db-Hsa.TEADΔN-2A-mCherry). Gal4db-Hsa.TEADΔN-2A-mCherry and Ola.sp7 promoter were sequentially inserted into the pTol2 vector.

To construct a pTol2-myl7:NLS-EGFP-HS4-UAS:EGFP-ytip, a DNA fragment encoding *NLS-mCherry* was removed from pTol2-myl7:NLS-mCherry-HS4-MCS vector and replaced with a cDNA fragment encoding *NLS-EGFP*. An upstream activating sequence (*UAS*) along with an E1b minimal promoter derived from pBluescript II-UAS:GFP vector was inserted to construct a pTol2-myl7:NLS-EGFP-HS4-UAS-MCS vector. Finally, a cDNA fragment encoding *ytip* was inserted into the pTol2-myl7:NLS-EGFP-HS4-UAS-MCS vector.

To construct a pTol2-cryaa:NLS-mCherry-HS4-UAS:EGFP-yap1-5SA plasmid, a myl7 promoter of a pTol2-myl7:NLS-mCherry-HS4-MCS vector was replaced by a cryaa promoter. A 5xUAS promoter derived from pTol2-5xUAS vector, a gift from K. Kawakami (National Institute of Genetics, Japan) (Asakawa et al., 2008; Distel et al., 2009), was subcloned to generate a pTol2-cryaa:NLS-mCherry-HS4-5xUAS-MCS vector. Finally, a cDNA fragment encoding *yap1-5SA* was inserted into the pTol2-

cryaa:NLS-mCherry-HS4-5xUAS-MCS vector. To construct a pEGFP-N1-Hsa.NPR3 plasmid, a *Hsa.NPR3* cDNA was inserted into the pEGFP-N1 vector. To construct a pCS3-npr2-EGFP plasmid, an *npr2* cDNA was inserted into the pEGFP-N1 vector. A cDNA fragment of *npr2-EGFP* was inserted into the pCS3 vector.

Transgenic (Tg) fish lines and knockout fish by a transcription activator-like effector nuclease (TALEN) method

The transgenic fish lines; *Tg(myl7:actn2-tdEos), Tg(myl7:ostn,hsp70l:EGFP), Tg(Hsa.RUNX2:GAL4FF-2A-mCherry), Tg(Ola.sp7:EGFP),Tg(Ola.sp7:GAL4FF-2A-mCherry), Tg(Ola.sp7:Gal4db-Hsa.TEAD2ΔN-2A-mCherry),* and *Tg(myl7:NLS-EGFP, UAS:EGFP-ytip)* fish lines were established by injecting Tol2-based plasmids (30 pg) with transposase mRNAs (25 pg) into the one-cell stage of wild type strain AB zebrafish embryos (Kawakami et al., 2004; Urasaki et al., 2006). Embryos were selected at 2-5 days post-fertilization (dpf) and grown to adults, among which germline founders were identified by promoter specific fluorescence expression. *Tg(myl7:NLS-mCherry)* fish line was reported previously (Fukui et al., 2014).

TALEN sequence against the second exon of *ostn* was designed using TAL Effector Nucleotide Targeter (Doyle et al., 2012). The *ostn* TALEN was generated using Golden Gate TALEN and TAL Effector Kit 2.0 (Addgene) (Cermak et al., 2011). The *ostn* TALEN recognition sequences are: 5'-TCTTGTCTGCTGACACTGACC-3' and 5'-CCGAAAGCCTTCACATA-3'. The sequence between the two binding sites contains a 16-bp spacer with a PstI site (TTGTTCCACTGCAGTG, PstI site underlined). TALEN mRNAs were *in vitro* transcribed from SacI-linearized expression plasmids with T3 RNA polymerase using a mMESSAGE mRNA kit (Ambion). A total of 200 pg TALEN mRNAs was microinjected into one-cell stage embryos. Mutant alleles were identified

by PstI digestion of a PCR product generated with the primers listed in the supplemental information (Table S1).

Chemicals, peptides, and antibodies

KT5823 was purchased from Calbiochem; synthetic human C-type natriuretic peptide (CNP) -22 from Peptide Institute; anti-YAP1/WWTR1 antibody (63.7) from Santa Cruz, Alexa Fluor 488-labeled secondary antibody and 4', 6-diamidino-2-phenylindole, dihydrochloride (DAPI) from Thermo Fisher Scientific; Streptavidin Cy3 conjugate, insulin, and 3-isobutyl-1-methylxathine (IBMX) were from Sigma-Aldrich. Mouse osteocrin (OSTN) (80-130 a.a.), rat (*Rattus norvegicus*) OSTN (82-132 a.a.), and biotin-labeled rat OSTN (82-132 a.a.) were synthetized by Sigma-Aldrich.

Microinjection of oligonucleotide and mRNA

For morpholino oligonucleotide (MO)-mediated gene knock down, embryos were injected at the one-cell stage with 4-10 ng of Control MO (Gene Tools), 8-15 ng of *ostn* splicing block MO (5'-CATTTCTTTATTTCACTACCTCTGC-3'), 3-5 ng of *npr2* splicing block MO (5'-AACCAAGAACACTCAACTCACCCCA-3'), and 4 ng of translation block *ctgfa* MO (5'-GAGTCATTCCAGAAAACATGATGAC -3'). The sequence of *ctgfa* MO has already been validated (Fukui et al., 2014).

Capped mRNAs were *in vitro* transcribed with SP6 RNA polymerase using a mMESSAGE mMACHINE kit (Ambion). For protein overexpression, one-cell stage embryos were injected with 100 pg of *EGFP* mRNA or 100 pg of *ctgfa* mRNA. For rescue experiment, one-cell stage embryos were coinjected with 4 ng of *npr2* MO and 160 pg of *npr2-EGFP* mRNA.

For EGFP-Yap1-5SA expression, one-cell stage of *Tg(Ola.sp7:GAL4FF-2A-mCherry)* embryos were injected with 30 pg of pTol2-cryaa-NLS-mcherry-HS4-5xUAS-EGFP-yap1-5SA plasmid. As a negative control, embryos were injected with 30 pg of pTol2-cryaa-NLS-mCherry-HS4-5xUAS-MCS plasmid and mCherry-positive embryos were selected for the experiment.

Fluorescence-activated cell sorting (FACS)

Hearts resected from the *Tg(myl7:NLS-mCherry)* or *Tg(myl7:actn2-tdEos)* larvae at 72 hours post-fertilization (hpf) were collected into a 1.5 ml tube, washed in phosphate buffered saline (PBS), and incubated with 1 ml of protease solution (PBS with 5 mg/ml trypsin and 1 mM EDTA, pH 8.0) for 1 h under occasional pipetting. Digestion of the hearts were terminated with 200 μl of stop solution (PBS with 30% fetal bovine serum [FBS] and 6 mM calcium chloride). The dissociated cells in suspension medium (phenol red free Dulbecco's modified Eagle's medium [DMEM, Life Technologies] with 1% FBS, 0.8 mM calcium chloride, 50 U/ml penicillin, and 0.05 mg/ml streptomycin) were subjected to cell sorting using a FACS Aria III cell sorter (BD Bioscience). mCherry- or tdEos-positive cells were collected as cardiomyocytes for further RNA preparation.

RNA preparation, RNA sequence (RNA-seq), and quantitative (q) RT-PCR

For RNA-seq, total RNAs were prepared from mCherry- or tdEos-positive cells using a NucleoSpin XS kit (Macherey-Nagel) according to the manufacture's instruction. Reverse transcription (RT) and cDNA library preparation were performed with a SMARTer Ultra Low RNA kit (Clontech). cDNA was fragmented with a Covaris S 220 instrument (Covaris). Subsequently, the sample was end-repaired, dA-tailed, adaptor ligated, and then subjected to PCR by using a NEBNext DNA Library Preparation and

NEBNext Multiplex oligos for Illumina (New England BioLabs). The sample was sequenced by using a MiSeq (Illumina) to generate pair-end 150-bp reads. Raw reads were mapped to zebrafish genome (DanRer7). Expression levels were measured by calculating reads per kilobase per million sequenced reads (RPKM) and normalized trimmed mean of M-values (TMM) method using an Avadis NGS software (Strand Life Sciences).

For RT-PCR, total RNAs were prepared from zebrafish larvae, mouse organs, or MC3T3-E1 cells using TRIzol reagent (Thrmo Fisher Scientific). RNAs were reverse-transcribed by random hexamer primers using SuperScript III (Thrmo Fisher Scientific) according to the manufacturer's instructions. PCR reactions was performed with TaKaRa Ex Taq Hot Start Version (TaKaRa) in a 2720 Thermal Cycler (Thrmo Fisher Scientific). For qRT-PCR, PCR reactions were performed with KOD SYBR qPCR Mix (TOYOBO) in a Mastercycler Realplex (Eppendorf). The primers used for RT-PCR and qRT-PCR were listed in supplementary data (Table S1).

Whole mount *in situ* hybridization (WISH)

Antisense *ostn*, *casr*, *myl7*, *myod1*, *sp7*, *sox9a*, *runx2a*, *runx2b*, *spp1*, *col10a1*, *npr2*, *npr3*, *nppcl*, and *ctgfa* RNA probes labeled with digoxigenin (DIG) were *in vitro* transcribed using an RNA labeling kit (Roche). WISH was performed according to the standard protocol as described previously (Fukui et al., 2014). Briefly, embryos and larvae were fixed in 4% paraformaldehyde (PFA) in PBS, dehydrated in methanol (MeOH), and gradually rehydrated into PBS containing 0.1% Tween 20 (PBS-T). For parasphenoid (ps) observation, larvae were resected the lower jaws. After digestion by PBS-T containing proteinase K (Roche) for 15-50 min, embryos and larvae were fixed

in 4% PFA and hybridized with antisense RNA probes at 65°C (*ostn*, *casr*, *myl7*, and *myod1* probes) or 70°C (the others) overnight in hybridization buffer (5 x SSC, 50% formamide, 5 mM EDTA, 0.1% tween20, 50 μg/ml heparin, and 1 mg/ml torula RNA). After hybridization, embryos and larvae were incubated with anti-DIG antibody conjugated with alkaline phosphatase (Roche) in blocking buffer at 4°C overnight. The colorimetric reaction was carried out using BM purple (Roche). Images of the embryos were recorded with a SZX16 Stereo microscope (Olympus).

Plastic section for ISH

Larvae hybridized with antisense *ostn*, *myod1*, *sp7*, and *sox9a* probe were dehydrate with acetone, embedded in Technovit 8100 (Heraeus Kulzer), and cut into 10 μm thick sections with a microtome (RM2125RT, Leica). Images of the sections were recorded with a BX51 microscope (Olympus).

Bone staining

Larvae at 5-10 dpf were fixed in PBS containing 4% PFA at 4°C overnight and stored in 100% MeOH at -20°C. For alizarin red staining, larvae were gradually rehydrated into water, bleached in 1.5% hydrogen peroxide in 1% potassium hydroxide (KOH) for 30 min, and washed in water. The bones were stained with 0.04 mg/ml Alizarin Red S in 1% KOH, destained with 20% glycerol in 1% KOH for 1 h, and stored in 50% glycerol in 0.25% KOH. For alcian blue staining, larvae were stained with 0.02% Alcian Blue 8GX in 70% ethanol (EtOH) containing 80 mM magnesium chloride ($MgCl_2$) at room temperature (RT) overnight, rehydrated into water, bleached in 1.5% hydrogen peroxide in 1% KOH for 30 min, and stored in 50% glycerol in 0.25% KOH. Cartilages were

dissected out, mounted in glycerol on slide glasses, and covered with cover slips. Bone images were recorded with a SZX16 Stereo microscope (Olympus) and the bone length was measured by a DP2-BSW software (Olympus). To detect the chondrocyte area, each chondrocyte was demarcated by drawing lines in the middle of cell border and measured the area inside of the lines.

To visualize live mineralized bone, larvae were incubated in 0.003% Alizarin red in 0.03% sea salt for 1 h. Confocal images were taken with a FV1000 confocal microscope system (Olympus) and the bone length was measured by Imaris software (Bitplane).

Measurement of head length

Embryos and larvae at 2-6 dpf were fixed in PBS containing 4% PFA at 4°C overnight, washed in PBS, and mounted in glycerol. Images were recorded with a SZX16 Stereo microscope (Olympus). The head length was measured by a DP2-BSW software (Olympus).

5-Ethynyl-2-deoxyuridine (EdU) assay

Larvae at 5 dpf were incubated in 200 μM EdU (Tokyo Chemical Industry). After 24 h incubation, larvae were fixed in 4% PFA at 4°C overnight and dehydrated with MeOH. Larvae were rehydrated into PBS-T, resected their brain by forceps, permeabilized by 0.5% triton X-100, blocked with 3% bovine serum albumin (BSA) at RT for 30 min, and stained with Click-iT EdU Alexa Fluor 647 Imaging Kit (Thermo Fisher Scientific) for 30 min. The quantification of EdU-positive cells were performed by using the images of the stained sections observed by a FV1000 confocal microscope (Olympus) and analyzed by IMARIS7.7.1 software (Bitplane).

TdT-mediated dUTP nick end labeling (TUNEL) assay

Larvae at 6 dpf were fixed in 4% PFA at 4°C overnight and dehydrated with MeOH. Larvae were rehydrated into PBS-T, resected the brain by forceps, digested by PBS-T containing proteinase K for 50 min at RT, and fixed in 4% PFA for 20 min at RT. After three times washing with PBS-T, larva were incubated with In Situ Cell Death Detection Kit, TMR red (Roche) for 60 min at 37°C. The quantification of TUNEL-positive cells were performed by using the images of the stained sections observed by a FV1000 confocal microscope (Olympus) and analyzed by IMARIS7.7.1 software (Bitplane).

Cell Culture, transfection, and siRNA-mediated knockdown

Murine MC3T3-E1 osteoblast-like cells were obtained from Riken BRC and cultured in minimum essential medium α (MEMα, Thrmo Fisher Scientific) with 10% FBS and antibiotics (100 mg/ml streptomycin and 100 U/ml penicillin). Human embryonic kidney HEK293T cells and Murine NIH3T3 fibroblast cells were cultured in DMEM (Nacalai Tesque) with 10% FBS and antibiotics. Murine ATDC5 chondrocyte cells were obtained from Riken BRC and cultured in a 1:1 mixture of DMEM and Ham's F-12 Nutrient Mixture (Nacalai Tesque) (DMEM/F12) with 5% FBS. HEK293T cells transfected with plasmids using polyethylenimine (PEI) max (Polyscience) were subjected to binding assay. MC3T3-E1 cells transfected with siRNAs from Thrmo Fisher Scientific (listed in supplementary Table S2) using Lipofectamine RNAi MAX reagents (Thrmo Fisher Scientific) were subjected to immunocytochemical analyses.

OSTN binding assay

Streptavidin conjugated Cy3 was diluted ten times and incubated with biotin, rat OSTN, or biotin-labeled rat OSTN on ice for 15 min to form OSTN-B–SA-Cy3. HEK293T cells transfected with pEGFP-N1-NPR3 or pEGFP-C1 empty vector (Clontech) and MC3T3-E1 cells were cultured for more than 24 h. HEK293T cells detached by pipetting using PBS and MC3T3-E1 cells treated by trypsin were resuspended with DMEM containing 10% FBS at $2x10^6$ cells/ml. After the incubation of cells with either CNP or unlabeled rat OSTN for 5 min, 0.1 μM OSTN-B–SA-Cy3 was added into the mixture and incubated for 30 min. The cells were washed with 15 ml PBS and resuspended in PBS containing 1% BSA, 0.2 mg/ml sodium azide, and SYTOX Blue Dead Cell Stain (Thrmo Fisher Scientific). Cy3 and EGFP fluorescence intensities were measured by FACS Aria III cell sorter (BD Bioscience). The data was analyzed using FACSDiva software (BD Bioscience).

Immunocytochemical analyses

MC3T3-E1 cells or ATDC5 cells were plated in 35-mm glass-base dishes (Asahi Techno Glass) coated with 1% gelatin. To examine the localization of YAP1/WWTR1, the cells were stimulated with human CNP for the time indicated in the figures in the presence or absence of mouse OSTN with or without a protein kinase G (PKG) inhibitor. After stimulation, the cells were fixed in PBS containing 4% PFA at RT for 15 min, permeabilized with 0.2% Triton X-100 at RT for 10 min, and blocked with PBS containing 3% BSA at RT for 1 h. The cells were immunostained with anti-YAP/WWTR1 antibody at RT for 2 h and visualized using Alexa Fluor 488-labeled secondary antibody. DAPI was used to counterstain nuclei. Fluorescence images of Alexa 488 and DAPI were recorded with a confocal microscope (FV1000, Olympus)

with 40x water objective lens (LUMPlanFL, FN 26.5, Olympus).

Measurements of intracellular cGMP

MC3T3-E1 cells, grown in 24 well plates, were incubated with incubation medium (DMEM containing 0.1% BSA and 500 μM IBMX) at 37°C for 30 min. The cells were subsequently stimulated with incubation medium containing 0.1-100 μM human CNP at 37°C for 15 min, replaced with ice cold 70% EtOH, and stored at -80°C. Cell lysates were transferred to test tubes, concentrated using a speedvac concentrator (Thermo scientific), and resuspended in 25 μl of double distilled water. The amount of cGMP in each cell lysate was measured using a cyclic GMP radioimmunoassay kit (Yamasa) according to the manufacturer's protocol.

Light sheet imaging

To record fluorescence in the beating heart, we used a lightsheet microscope (Lightsheet Z.1, Carl Zeiss). Larvae were anesthetized in 0.016% tricaine in 0.03% sea salt and transferred into 50 μl glass capillaries with 1% low-melting agarose dissolved in 0.03% sea salt. Images were processed with a ZEN2012 software (Carl Zeiss).

Bright field movie

To record bright field movies of larvae heart beating of, we used a SZX16 Stereo microscope (Olympus). Images were processed with a DP2-BSW software (Olympus).

Supplementary table S1. Primers used for genotyping, cassette amplification, RT-PCR, and qRT-PCR.

Primer Name	Sequence (5'-3')
For genotyping	
ostn-gTAL-fw	ATGCTGGGCTGTGGATGTGTGCT
ostn-gTAL-rev	CAGAGGCTCTCTAGGGGAAA
For RT-PCR and qPT-PCR	
ostn(Dr)-fw	CTGACACTGACCTTGTTCCACT
ostn(Dr)-rev	TACACCAATCCGGTCAATCG
eef1a1l1(Dr)-fw	AACCCCAAGGCTCTCAAATC
eef1a1l1 (Dr)-rev	GCACAGCAAAGCGACCAAG
npr2(Dr)-fw	GACAGCCCTGAGTATACCGC
npr2(Dr)-rev	TGCACGGAGAGAATCCACAG
sp7(Dr)-fw	TCCAGACCTCCAGTGTTTCC
sp7(Dr)-rev	ATGGACATCCCACCAAGAAG
col10a1(Dr)-fw (+77)	AGAAGGTGATGAAGGCCCCGCAGTAC
col10a1(Dr)-rev (+217)	CACCATCTTGTCCTGCAGGTCCAGGT
Ctgf(Mm)-fw	ATTTGGCCCAGACCCAACTA
Ctgf(Mm)-rev	GGCTCTGCTTCTCcAGtCTG
Npr2(Mm)-fw	TTTCCGGAAGCTGATGCTG
Npr2(Mm)-rev	TGACCGGTGTTGGCAAAGAT
Npr3(Mm)-fw	GAAGTACTCAGAGCTGGCTACAGCA
Npr3(Mm)-rev	CCTGCTTCAGTGTCAGTCATGGCAA
Actb(Mm)-fw	GTGACGTTGACATCCGTAAAGA
Actb(Mm)-rev	GCCGGACTCATCGTACTCC
For Cloning	
XhoI-*actn2*(Dr)-fw	CTCGAGATGATGAATCAGATCGAGCTTTCAGT GCCT
Asp718-*actn2*(Dr)-rev	GGTACCGTAAGGTCACTTTCTCCATATAGGGC

	GGTGGAG
PacI-*ostn*(Dr)-fw	TTAATTAACAGATTAAGGATGCTGGGCTGTGG AT
PacI-*ostn*(Dr)-rev	TTAATTAAACCTGCAATATTCCCCTGTATTTGC C
BamHI-*casr*(Dr)-fw	GGATCCTGGGTCTTTTCTACATCCCTCAGA
casr(Dr)-rev	GTCTTTAAAGCCGGGTATATGTCC
BamHI-*myod1*(Dr)-fw	GGATCCAAGATGGAGTTGTCGGATATCC
myod1(Dr)-rev	AGAATTTTAAAGCACTTGATAAATGG
Sox9a(Dr)-fw	GCGAGCTGAGCAGCGATGTT
Sox9a(Dr)-rev	GCATGCAAATTAAGTAGAAC
BamHI-*spp1*(Dr)-fw	GGATCCGGACCAGGCAGCTACAGAAG
spp1(Dr)-rev	CACTGCCGTCTGTCGTCTAA
BamHI-*npr2*(Dr)-fw	GGATCCATTGTGCTGCTTACACGCATGGTCG
npr2(Dr)-rev	CATTCCACTGGATATCTGAACCCTG
BamHI-*npr2*(Dr)-fw (-14)	GGGATCCTTTGCCAACATAAGATGGGATCGCT
npr2(Dr)-rev (+1652)	GCCACCAGGTTGCCCTTAAAATAGC
npr2(Dr)-fw (+1526)	ATCACAAGCGTGCAGGAAGCC
NheI-*npr2*(Dr)-rev (+1652)	GCTAGCCCTGGCATCAACAGTGCTCTCA
npr3(Dr)-fw	ATGTCATGTTTCATGCCACTCTGTCTGTCC
npr3(Dr)-rev	CTACGCTGCTGAAAAGTTGGATCTGATGGA
BamHI-*nppcl*(Dr)-fw	GGATCCCTGACCCAGAATCAGCATCTCCA
nppcl(Dr)-rev	ATCCGCACTCGATGACGTCTGTG
sp7(Dr)-fw	TTAGACATGACGCATCCTTACG
sp7(Dr)-rev	CGTTGCCTGTGCTGCTCTTTTC
runx2a (Dr)-fw	CCACGCCGAACTCCTTCAATC
runx2a (Dr)-rev	TCAATATGGCCGCCACACGGA

runx2b (Dr)-fw	ATGCGCATTCCCGTAGATCC
runx2b (Dr)-rev	TCAATACGGCCTCCAAACGCC
col10a1(Dr)-fw (+1326)	TGGCCCAGCAGGTCCTGGAGGCCCA
col10a1(Dr)-rev (+1772)	TTATAAAGTGCCACTAAAGCATTAG
SalI-*Ostn*(Mm)-fw	GTCGACATGCTGGACTGGAGATTGGCA
NotI-*Ostn*(Mm)-rev	GCGGCCGCTCAGCCTCTGGAACTGGAGAGCC GGTT
NheI-*NPR3*(Hs)-fw	GCTAGCATGCCGTCTCTGCTGGTGCTCACTTT CTCC
BamHI-*NPR3*(Hs)-rev	GGATCCCGAGCTACTGAAAAATGGGATCTGAT GGAATC

Supplementary table S2. siRNAs used for knockdown.

siRNA Name	Sequence (5'-3')
NPR2#1	TAGCACTTCGAAGTGGTCCTTTCTA
NPR2#2	CAGCCCATGGGAAATACCAGATCTT

Supplementary Figures

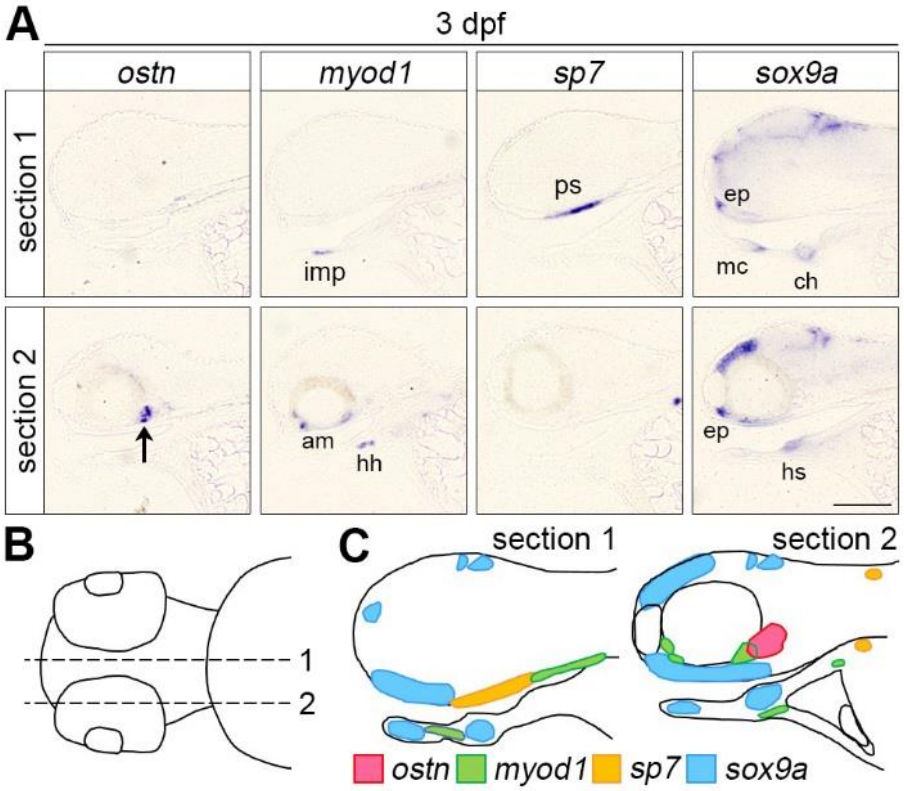

Fig. S1. *osteocrin* (*ostn*) mRNA in the head. (**A**) Whole mount *in situ* hybridization (WISH) analyses of mRNAs indicated at the top in the larvae at 3 days post-fertilization (dpf). Sagittal sections of midline (upper panels, section 1) and the *ostn* expressing area (lower panels, section 2), anterior to the left. The arrow indicates *ostn* mRNA expression. imp, intermandibularis posterior; am, adductor mandibulae; hh, hyohyoideus; ps, parasphenoid; ep, ethmoid plate; mc, meckel's cartilage; ch, ceratohyal; hs, hyosymplectic. Scale bar, 100 μm. (**B**) Schematic drawing of the zebrafish head at 3 dpf, ventral view, anterior to the left. Broken lines indicate the planes of section 1 (upper line) and section 2 (lower line). (**C**) Schematic drawing of the expression of mRNAs indicated at the bottom. Section 1 (left) and section 2 (right), anterior to the left.

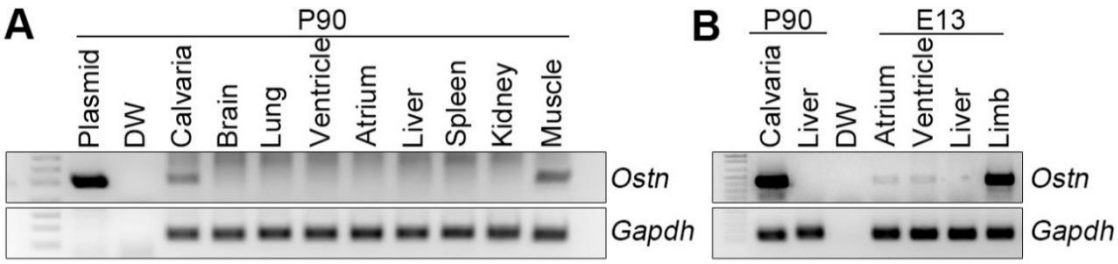

Fig. S2. *ostn* mRNA expression in the mouse organs. (**A**) Representative results of reverse transcription (RT)-PCR analyses of *Ostn* (upper panel) and *Gapdh* (lower panel) mRNAs in postnatal day 90 (P90) mouse organs indicated at the top. pCR4-Mmu.Ostn (Plasmid) and distilled water (DW) were used as a positive and a negative control, respectively. (**B**) RT-PCR analyses of embryonic day 13 (E13) mouse organs indicated at the top. P90 mouse organs and DW were used as controls.

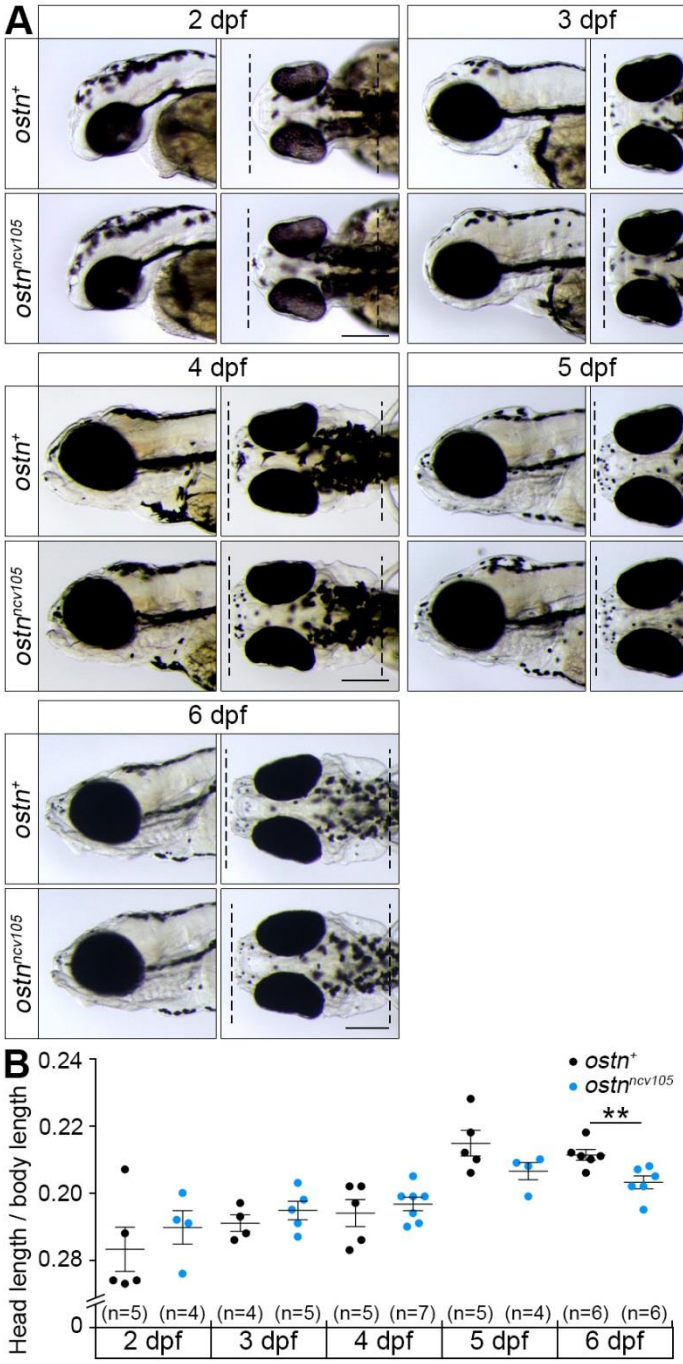

Fig. S3. Head morphology and length of *ostn* mutants. (**A**) Representative images of the head of the 2-6 dpf wild type (upper panels) and homozygous mutant (lower panels) embryos and larvae. Lateral view (left panels) and dorsal view (right panels), anterior to the left. Broken lines indicate the tip and the end of the heads. (**B**) The ratio of the head length (from the tip of the head to the center of hourglass like shape at the back of the head) to the body length (from the tip of the upper jaw to the end of the tail) of wild type (*ostn*$^{+}$) or homozygous mutant (*ostn*^{ncv105}) larvae at 2-6 dpf. The data were analyzed by Student's *t*-test. Statistical significance, **p < 0.01. Error bars indicate s.e.m. Scale bars, 200 μm.

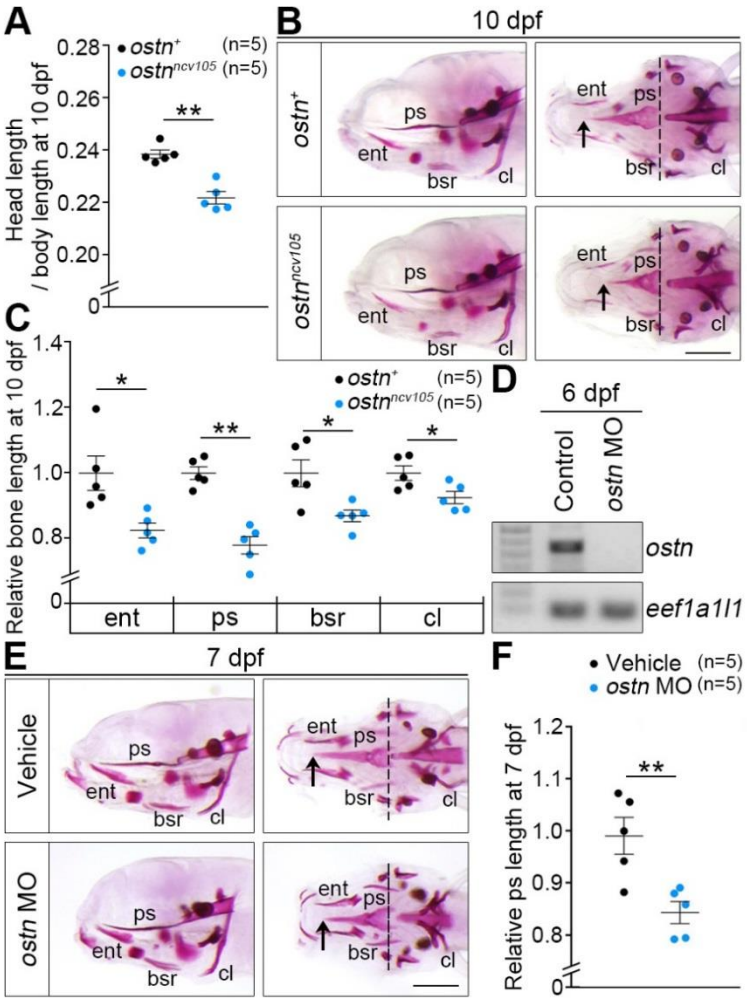

Fig. S4. Depletion of Ostn results in shortening of the ps and other intracranial membranous bones. (**A**) The ratio of the head length to the body length of the 10 dpf wild type (*ostn*$^{+}$) or homozygous mutant (*ostn*^{ncv105}) larvae was analyzed similarly to Fig. 3C. (**B**) Representative images of alizarin red staining of the 10 dpf larvae of wild type (upper panels) and homozygous mutant (lower panels). Lateral view (left panels) and ventral view (left panels), anterior to the left. Arrows and broken lines indicate the tip and the top of the concave in the caudal part of the parasphenoid, respectively. ent, entopterygoid; ps, parasphenoid; bsr, branchiostegal ray; cl, cleithrum. (**C**) Quantitative analyses of (B). Each relative bone length to the mean length of wild type bones was plotted. The length of ps was measured similarly to Fig. 3E. (**D**) A representative result of RT-PCR analyses of *ostn* (upper panel) and *eef1a1l1* (lower panel) mRNAs of the larvae injected with control morpholino oligonucleotide (MO) and *ostn* MO at 6 dpf. (**E**) Representative images of alizarin red staining of the 7 dpf larvae injected with vehicle (upper panels) and *ostn* MO (lower panels). Lateral view (left panels) and ventral view (left panels), anterior to the left. (**F**) Quantitative analyses of (E). The data were analyzed by Student's *t*-test. Statistical significance, *p < 0.05; **p < 0.01. Error bars indicate s.e.m. Scale bars, 200 μm.

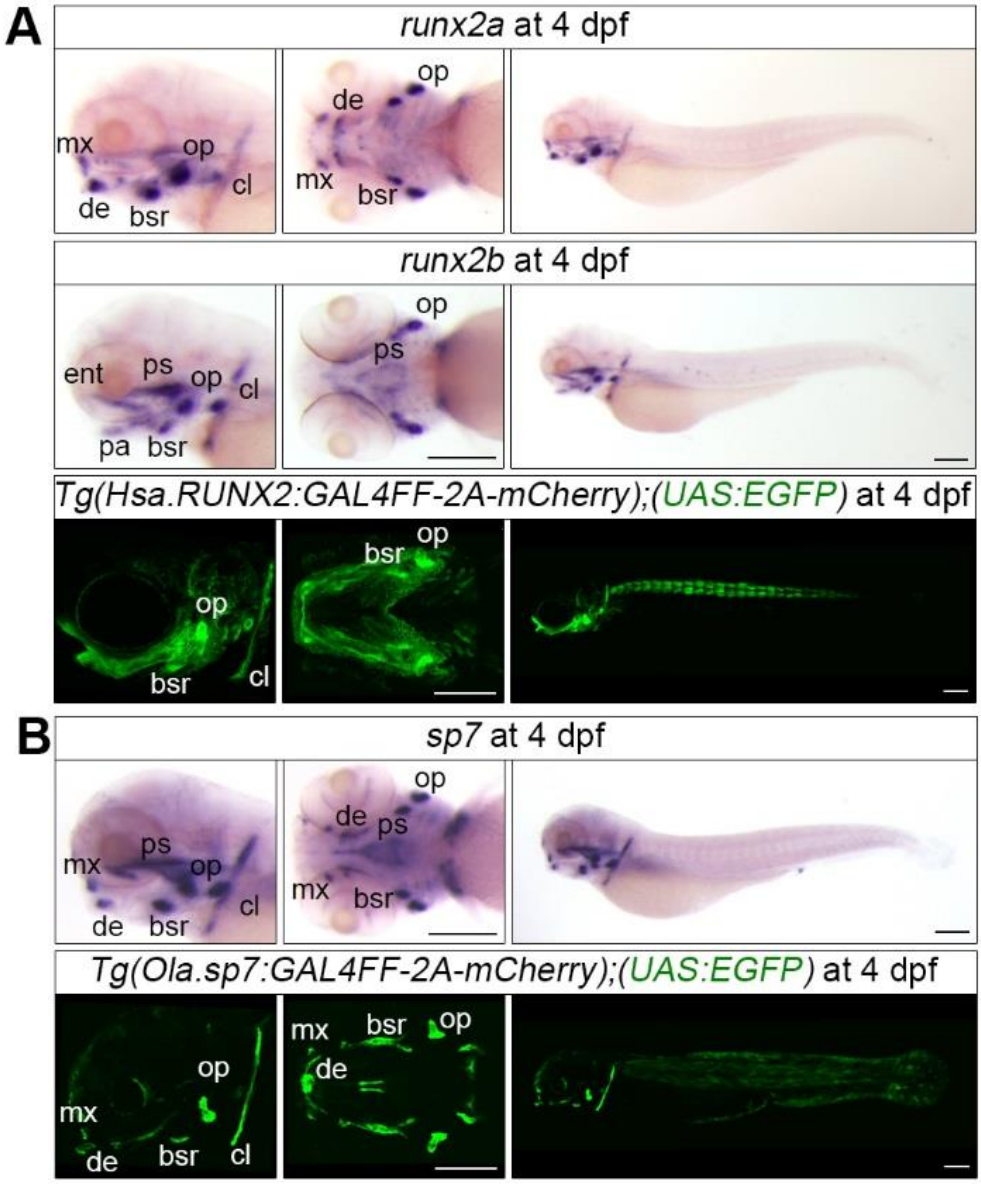

Fig. S5. The EGFP reporter expression reflects endogenous *runx2a/b* and *sp7* mRNA expression. (**A**) WISH analyses of *runx2a* (upper panels) and *runx2b* mRNAs (middle panels) in the larvae at 4 dpf. Projection views of confocal images of EGFP reporter expression in a Tg*(Hsa.RUNX2:GAL4FF-2A-mCherry);(UAS:EGFP)* (bottom panels) larva at 4 dpf. Lateral view of the head (left panels), ventral view of the head (center panels), and lateral view of the whole body (right panels), anterior to the left. (**B**) WISH analysis of *sp7* mRNA expression (upper panels) in a larva at 4 dpf. Projection views of confocal images of EGFP reporter expression in a *Tg(Ola.sp7:GAL4FF -2A-mCherry);(UAS:EGFP)* (bottom panels) larva at 4 dpf. Lateral view of the head (left panels), ventral view of the head (center panels), and lateral view of the whole body (right panels), anterior to the left. mx, maxilla; de, dentary; pa, pharyngeal arches; ent, entopterygoid; ps, parasphenoid; bsr, branchiostegal ray; op, opercle; cl, cleithrum. Scale bars, 200 μm.

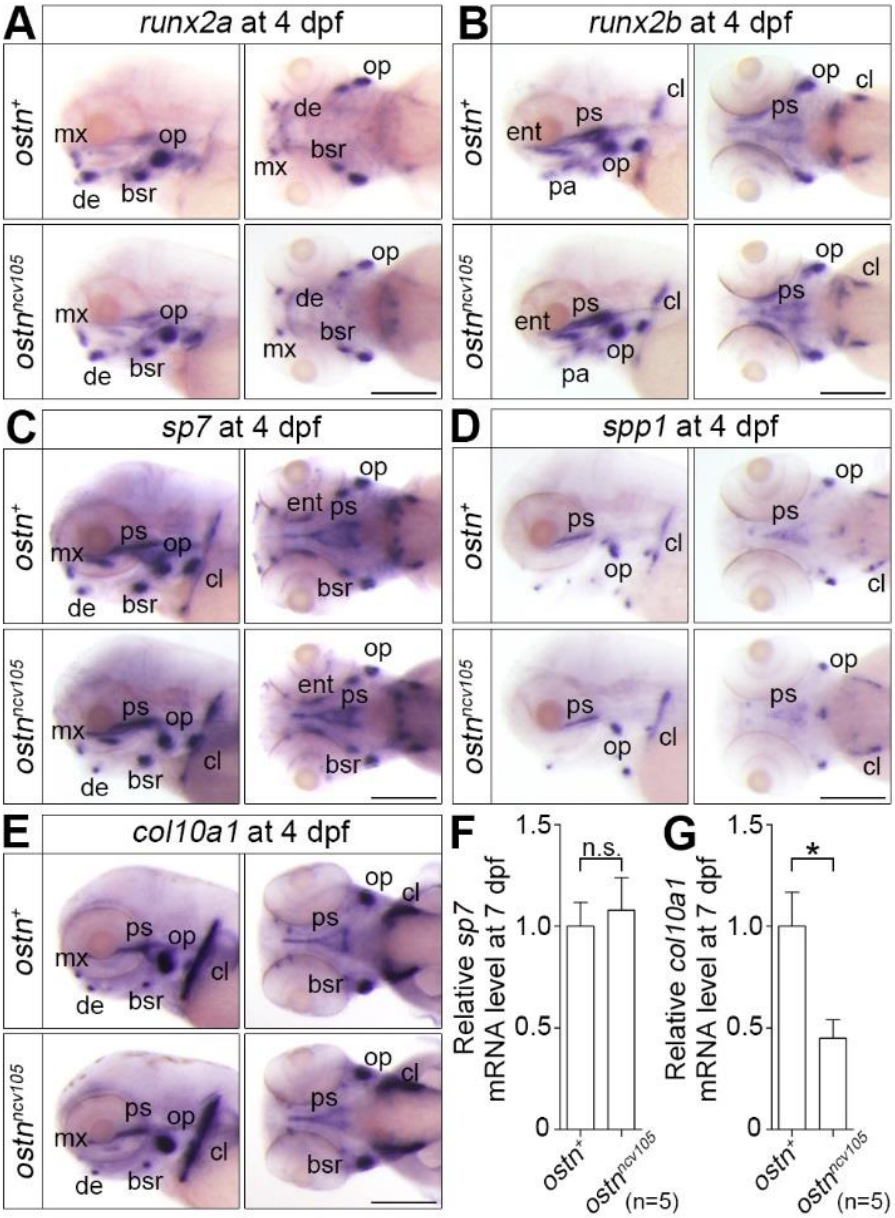

Fig. S6. ECM expression was reduced in *ostn* mutant. (**A-E**) WISH analyses of *runx2a* (A), *runx2b* (B), *sp7* (C), *spp1* (D), and *col10a1* mRNAs (E) in the 4 dpf larvae of wild type (upper panels) and *ostn*^{ncv105} mutant (lower panels). Lateral view (left panels) and dorsal view (right panels), anterior to the left. mx, maxilla; de, dentary; pa, pharyngeal arches; ent, entopterygoid; ps, parasphenoid; bsr, branchiostegal ray; op, opercle; cl, cleithrum. (**F, G**) qRT-PCR analyses of *sp7* (F) and *col10a1* (G) mRNAs of wild type (*ostn*$^{+}$) or homozygous mutant (*ostn*^{ncv105}) larvae at 7 dpf. The data were analyzed by Student's *t*-test. Statistical significance, *p < 0.05; n.s., no significance between two groups. Error bars indicate s.e.m. Scale bars, 200 μm.

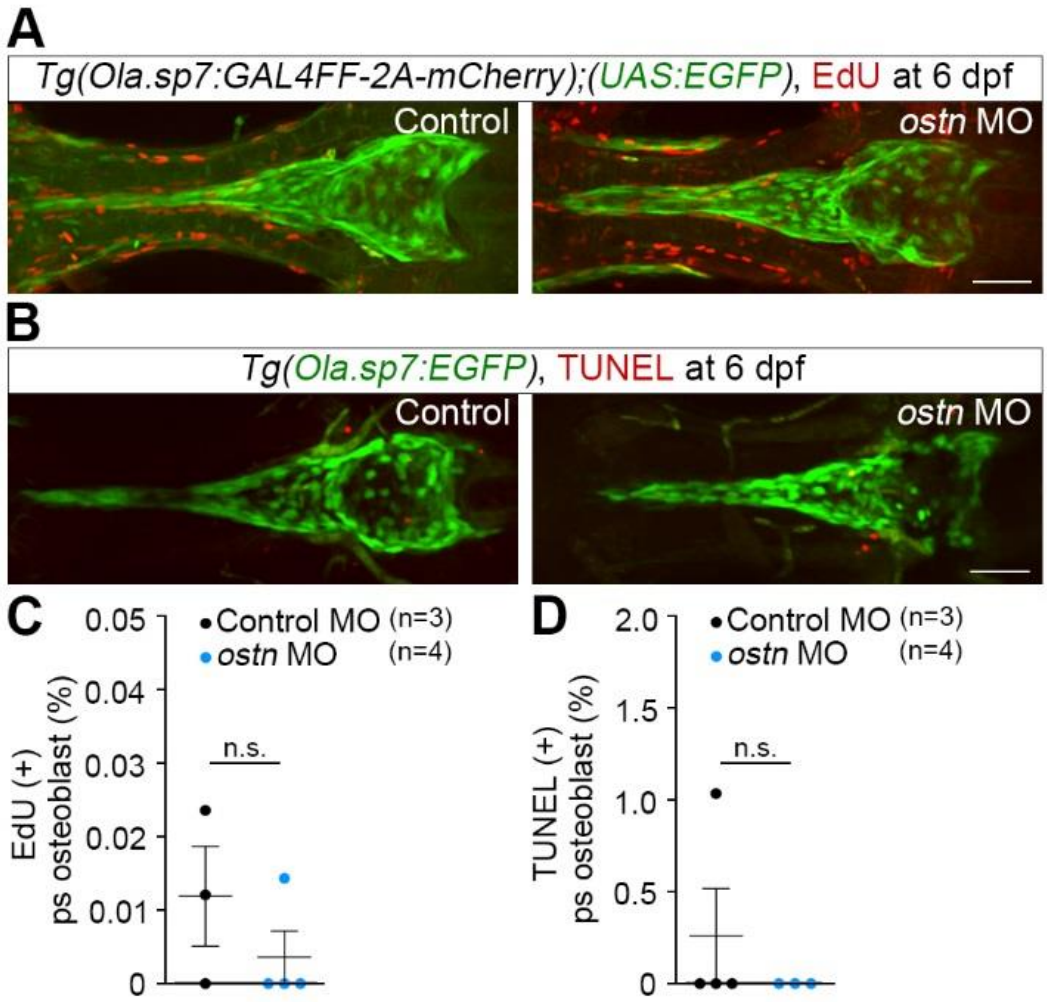

Fig. S7. Osteoblast proliferation and apoptosis were comparable between the *ostn* mutant and control larvae. (**A**) Representative confocal images of 5-ethynyl-2-deoxyuridine (EdU) incorporation (red) in the ps of the *Tg(Ola.sp7:GAL4FF-2A-mCherry);(UAS:EGFP)* larvae at 6 dpf injected with control MO (left panel) and *ostn* MO (right panel). EdU-positive cells are marked by red. (**B**) Representative confocal images of TdT-mediated dUTP nick end labeling (TUNEL) staining (red) in the ps of the *Tg(Ola.sp7:EGFP)* larvae at 6 dpf injected with control MO (left panel) and *ostn* MO (right panel). (**C**) Quantitative analyses of EdU-positive percentage of EGFP-positive osteoblasts in the ps. (**D**) Quantitative analyses of (B). The data were analyzed by Student's *t*-test. n.s., no significance between two groups. Error bars indicate s.e.m. Scale bars, 50 μm.

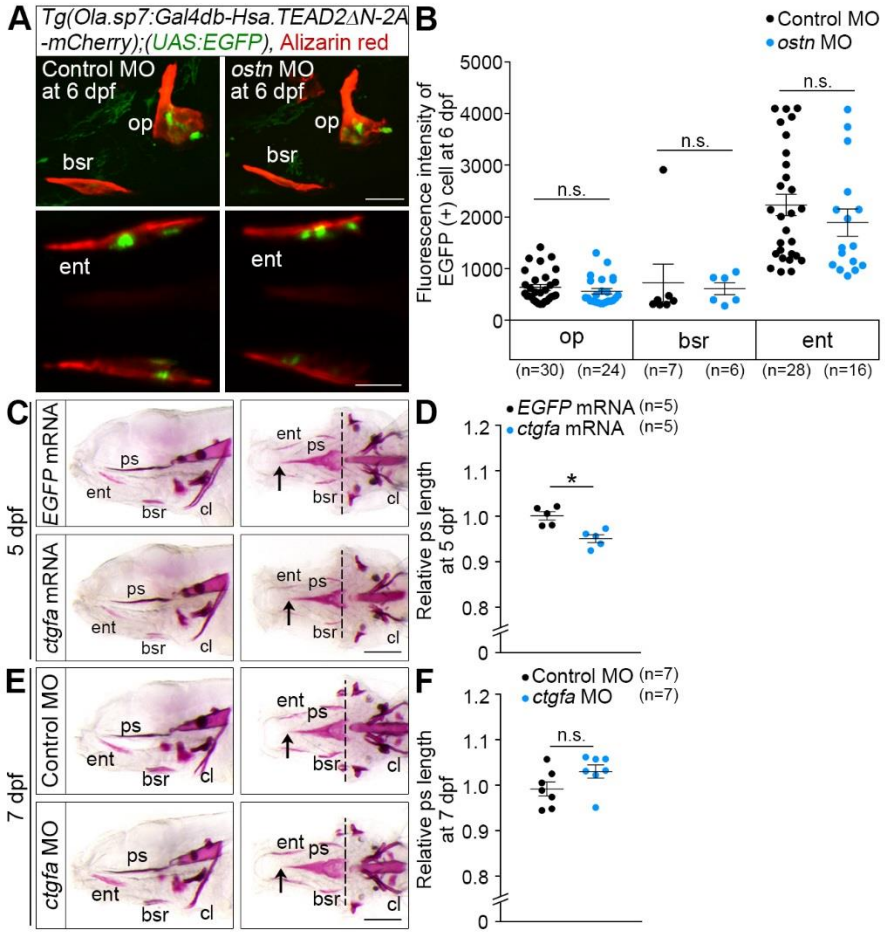

Fig. S8. Ctgfa affects the ps formation. (**A**) Representative confocal images of the op, bsr (upper panels), and ent (lower panels) of the *Tg(Ola.sp7:Gal4db-Has.TEAD2deltaN-2A-mCherry);(UAS:EGFP)* larvae injected with control MO (left panels) or *ostn* MO (right panels) and stained with alizarin red at 6 dpf. ent, entopterygoid; bsr, branchiostegal ray; op, opercle. (**B**) Quantitative analyses of (A). The intensity of EGFP-positive area in each bone was plotted. The number of EGFP-positive area was indicated at the bottom. (**C**) Representative images of alizarin red staining of the 5 dpf larvae injected with *egfp* mRNA (upper panels) and *ctgfa* mRNA (lower panels). Lateral view (left panels) and ventral view (left panels), anterior to the left. Arrows and broken lines indicate the tip and the top of the concave in the caudal part of the ps, respectively. ps, parasphenoid; cl, cleithrum. (**D**) Quantitative analyses of (C). The length of the ps was measured similarly to Fig. 3E. (**E**) Representative images of alizarin red staining of the 7 dpf larvae injected with control MO (upper panels) and *ctgfa* MO (lower panels). Lateral view (left panels) and ventral view (right panels), anterior to the left. (**F**) Quantitative analyses of (E). The data were analyzed by Student's *t*-test. Statistical significance, *p < 0.05. n.s., no significance between two groups. Error bars indicate s.e.m. Scale bars, 50 μm (A) and 200 μm (C and E).

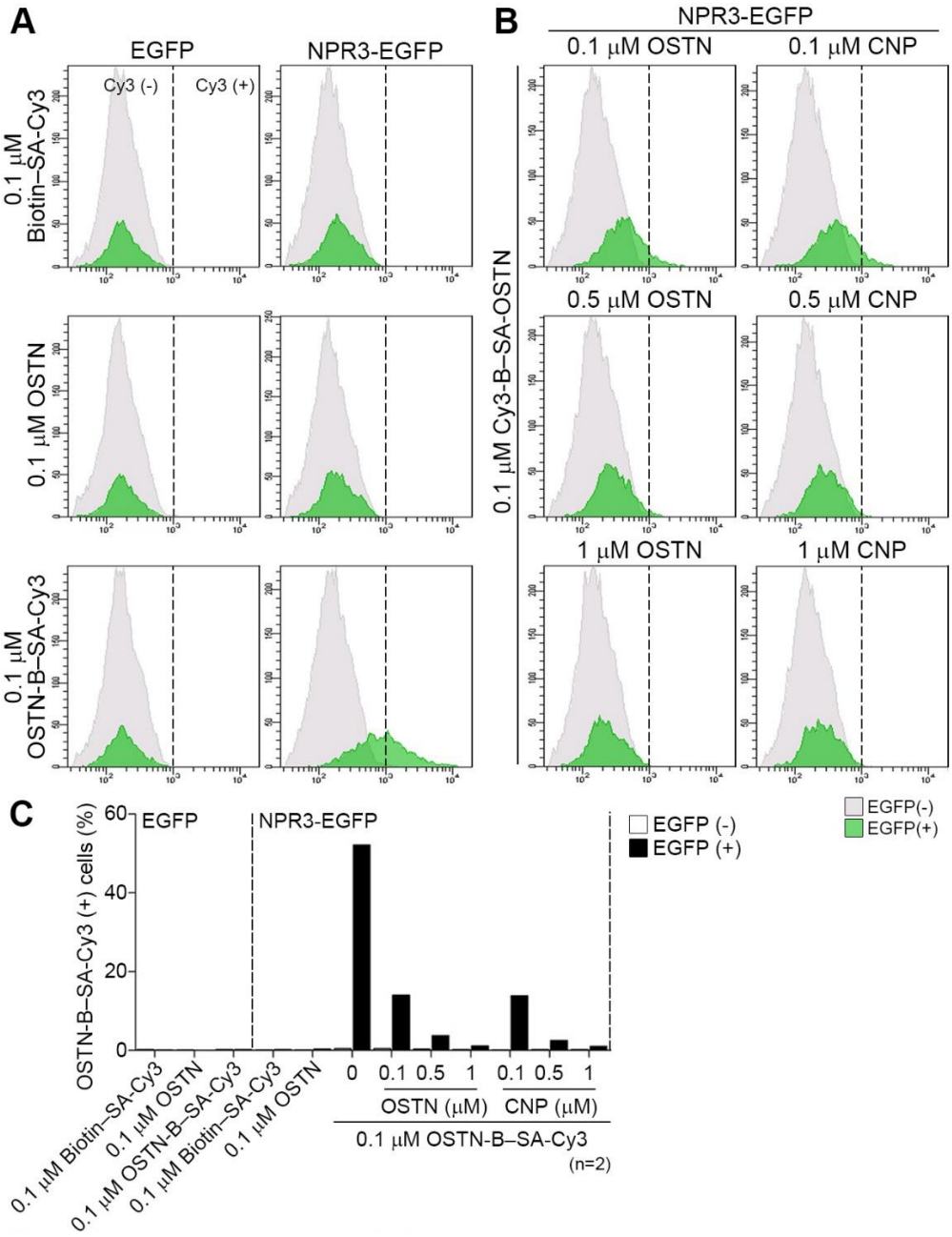

Fig. S9. OSTN and CNP competitively bind to NPR3. (**A**) Binding of biotin (top panels), unlabeled rat OSTN (middle panels), or biotin-labeled rat OSTN (OSTN-B) (bottom panels) to EGFP (left panels) or NPR3-EGFP (right panels) overexpressed in HEK293T cells was analyzed by flow cytometry. Binding of OSTN-B was detected by Cy3-conjugated streptavidin (SA-Cy3). (**B**) Binding of OSTN-B to NPR3-EGFP overexpressed in HEK293T cells in the presence of unlabeled rat OSTN (right panels) or human CNP (left panels) at the dose indicated on the top was analyzed similarly to (A). Note that binding of OSTN-B to NPR3-EGFP was inhibited by either unlabeled rat OSTN or human CNP. (**C**) Quantitative analyses of (A) and (B).

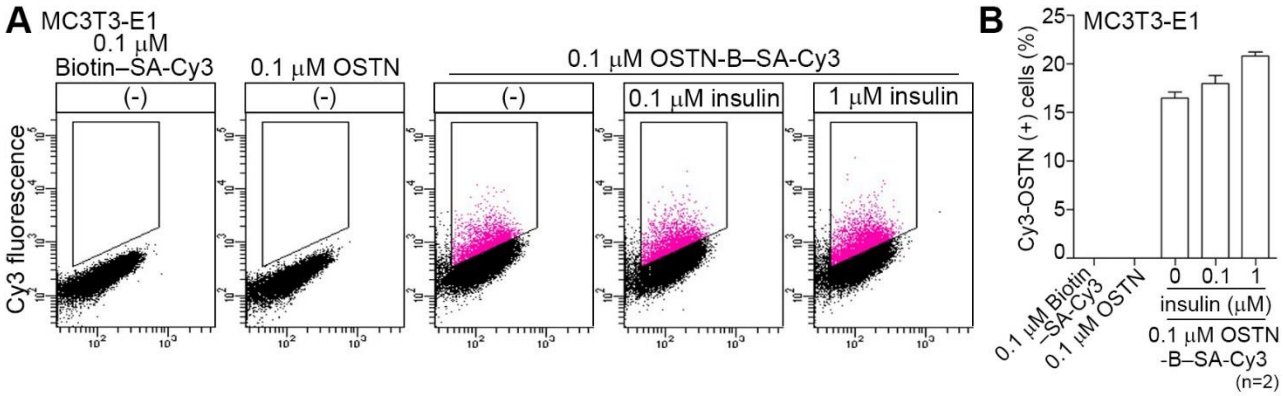

Fig. S10. Binding of OSTN to NPR3 is not affected by insulin. (**A**) Competitive binding of biotin-labeled rat OSTN with insulin to MC3T3-E1 cells was analyzed by flow cytometry. The binding of OSTN-B in the presence of insulin indicated at the top to MC3T3-E1 cells was shown as a dot-plot data. (**B**) Quantitative analyses of (A). Error bars indicate s.e.m.

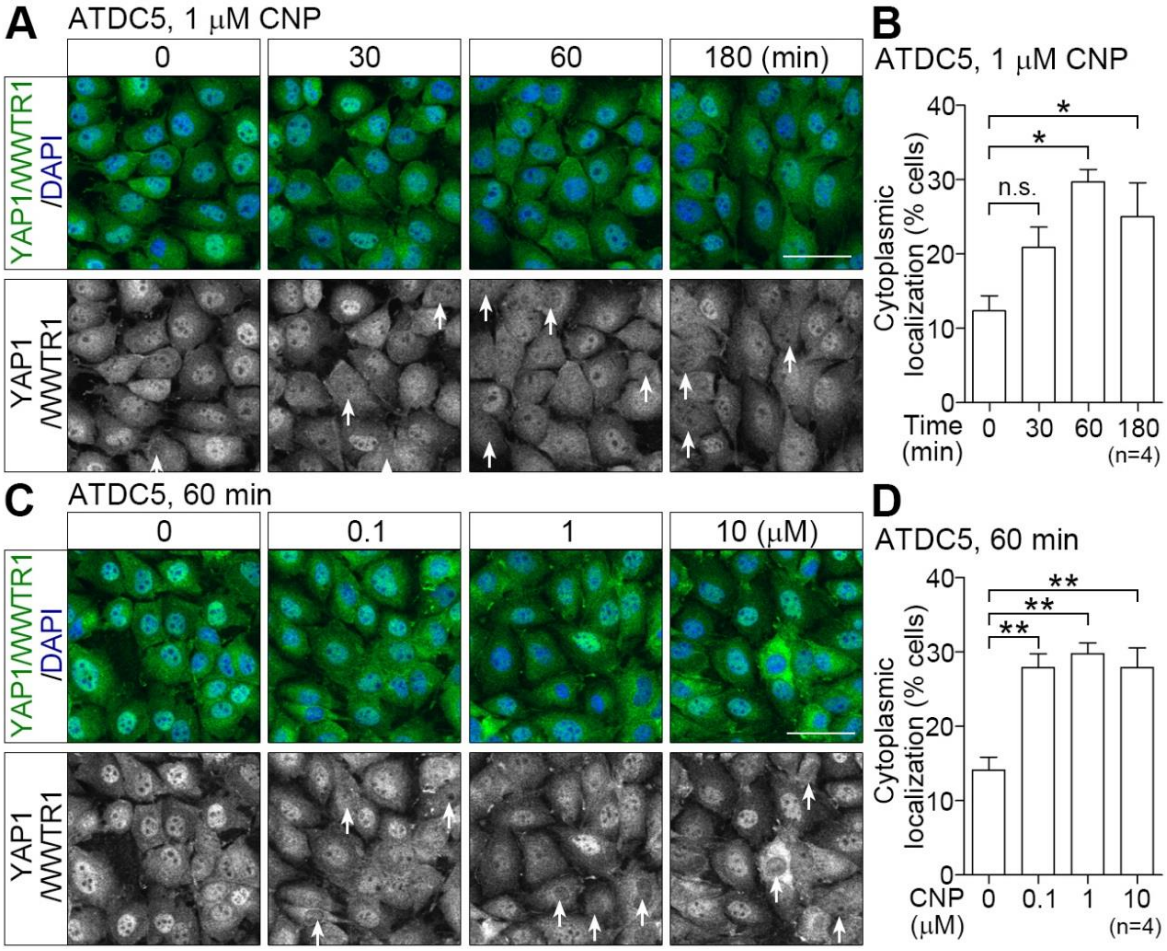

Fig. S11. CNP induces nuclear export of YAP1/WWTR1 in ATDC5 cells. (**A**) Representative images of immunostaining of ATDC5 cells stimulated with 1 μM CNP for the time indicated at the top with anti-YAP1/WWTR1 antibody and DAPI. Double staining of DAPI (blue) and YAP1/ WWTR1 (green) (upper panels) and YAP1/WWTR1 staining displayed in gray-scale image (lower panels). Arrows indicate the cells exhibiting nuclear export of YAP1/WWTR1. (**B**) Quantitative analyses of nuclear export of YAP1/WWTR1 in (A) were analyzed similarly to Fig. 6D. (**C**) Representative images of immunostaining of ATDC5 cells stimulated for 60 min with CNP at the dose indicated at the top with anti-YAP1/WWTR1 antibody and DAPI. (**D**) Quantitative analyses of nuclear export of YAP1/WWTR1 in (D) were analyzed similarly to Fig. 6D. The data were analyzed by one-way ANOVA with Turkey's test. Statistical significance, *$p < 0.05$; **$p < 0.01$. n.s., no significance between two groups. Error bars indicate s.e.m. Scale bars, 50 μm.

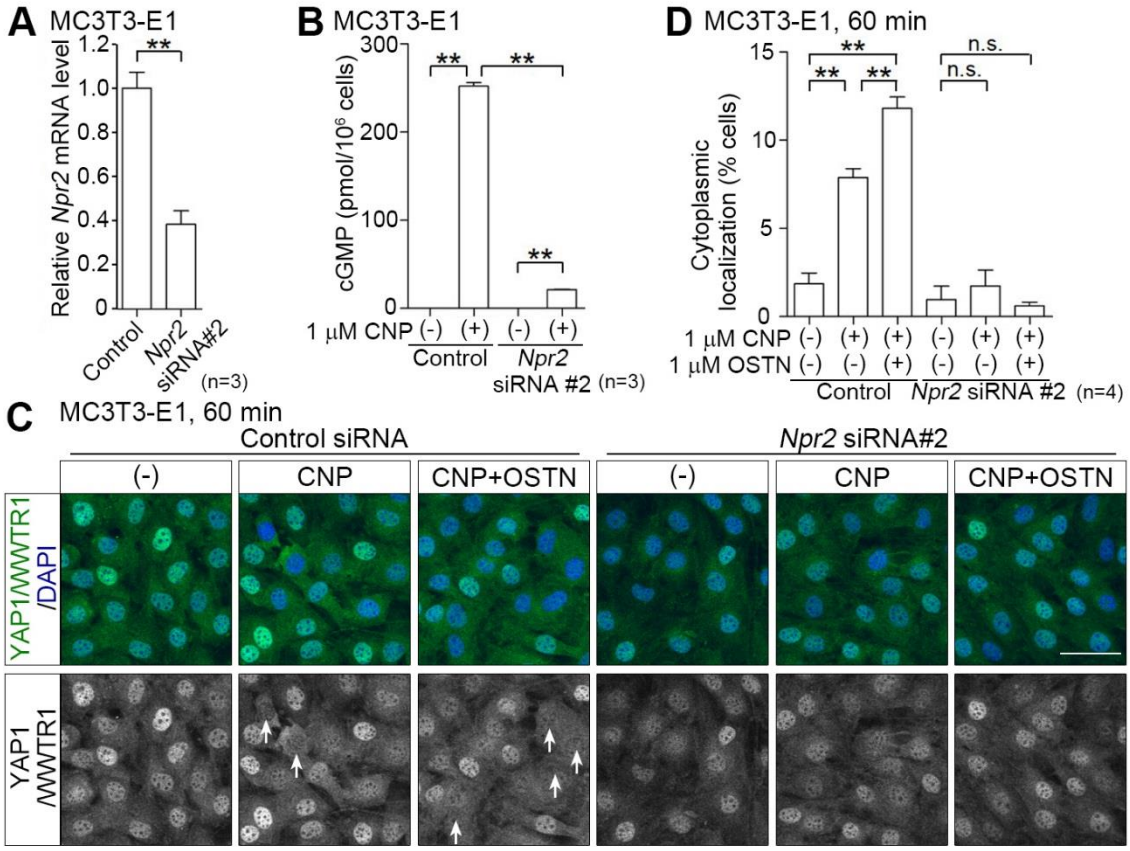

Fig. S12. Npr2 siRNA#2 pretreatment reduces CNP-induced nuclear export of YAP1/WWTR1. (**A**) qRT-PCR analyses of *Npr2* mRNA of MC3T3-E1 cells treated with siRNA against *Npr2* for 72 h to validate the knockdown efficiency of siRNAs. (**B**) Measurement of cGMP in MC3T3E1 cells pretreated with siRNAs for 72 h and stimulated with 1 μM CNP for 15 min as indicated at the bottom. (**C**) Representative images of Immunostaining of MC3T3-E1 cells pretreated with either control siRNA (left three panels) or *Npr2* siRNA#2 (right three panels) and simulated with peptide (1 μM CNP and/or 1 μM OSTN) as indicated at the top with anti-YAP1/WWTR1 antibody. (**D**) Quantitative analyses of the nuclear exports of YAP1/WWTR1 of the cells in (C) were analyzed similarly to Fig. 6D. The data were analyzed by Student's *t*-test or one-way ANOVA with Turkey's test. Statistical significance, $^{**}p < 0.01$. n.s., no significance between two groups. Error bars indicate s.e.m. Scale bar, 50 μm.

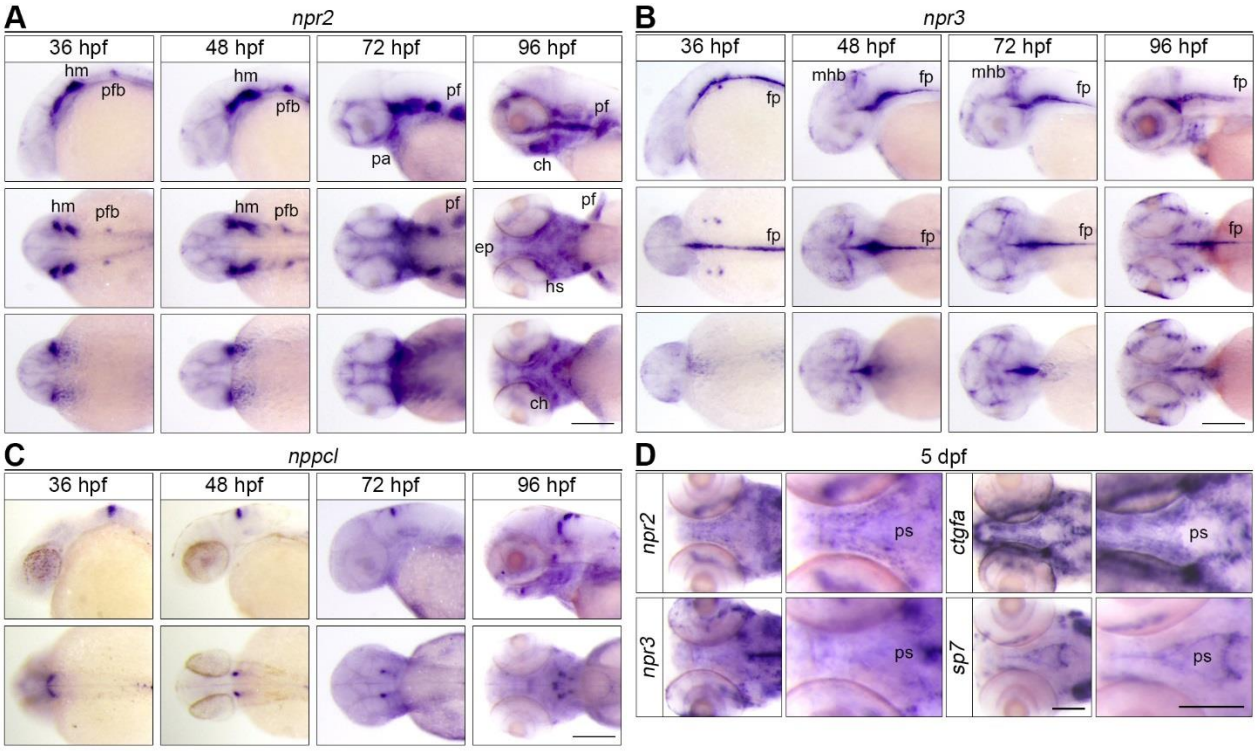

Fig. S13. The expression of *npr2*, *npr3* and *nppcl* mRNAs. (**A-B**) WISH analyses of *npr2* (A) and *npr3* (B) mRNAs of the larvae at the time point indicated at the top. Lateral view (upper panels), dorsal view (middle panels), and ventral view (left panels), anterior to the left. hm, head mesenchyme; pfb, pectoral fin bud; pa, pharyngeal arches; pf, pectoral fin; ch, ceratohyal; ep, ethmoid plate; fp, floor plate; mhb, midbrain hind brain boundary. (**C**) WISH analyses of *npplc* mRNA of the larvae at the time point indicated at the top. Lateral view (upper panels), dorsal view (lower panels), anterior to the left. (**D**) WIHS analyses of mRNAs indicated at the left of the ps area in the 5 dpf larvae resected the lower jaw. Ventral view of the head (left panels) and high magnification image (right panels), anterior to the left. *sp7* mRNA expression is a positive control to show the ps. Scale bars, 200 μm.

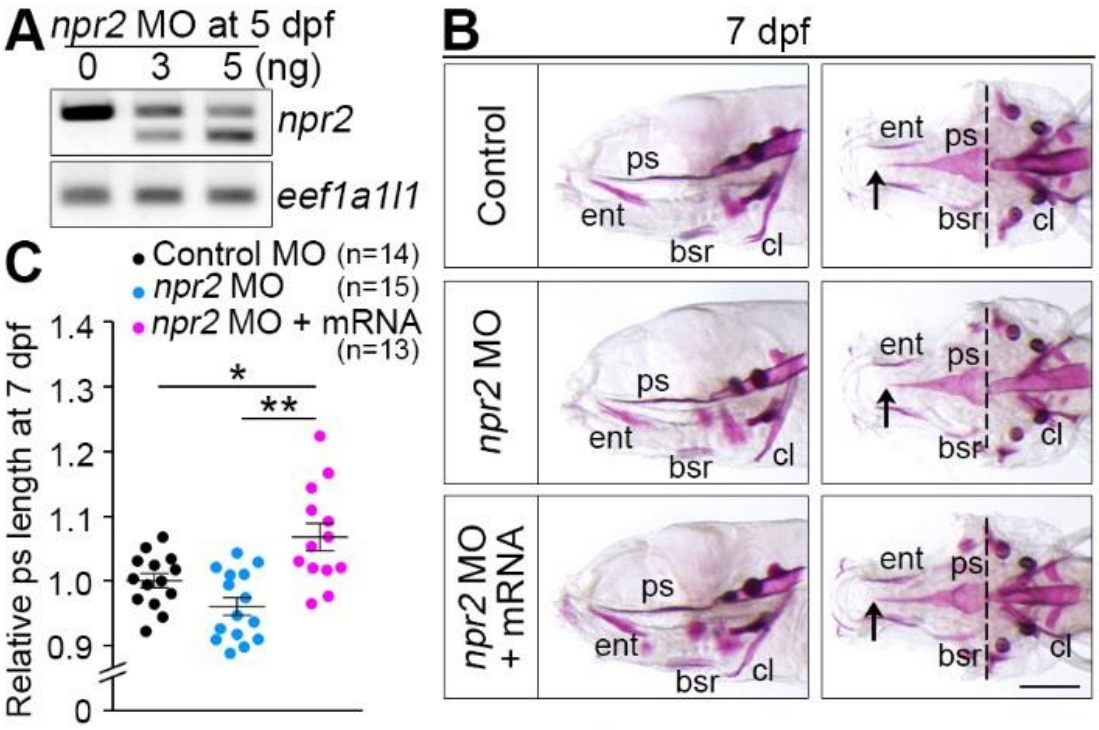

Fig. S14. Validation of the *npr2* MO. (**A**) Representative RT-PCR analyses of *npr2* (upper panel) and *eefa1a1l1* (lower panel) mRNAs of the 5 dpf larvae injected with vehicle (left), 3 ng *npr2* MO (center), and 5 ng *npr2* MO (right). MO injection resulted in shorter PCR products. (**B**) Representative images of alizarin red staining of the 7 dpf larvae injected with control MO (top), 5 ng *npr2* MO (middle), and 5 ng *npr2* MO with 160 pg *npr2-EGFP* mRNA (bottom). Lateral view (left panels) and ventral view (right panels), anterior to the left. ent, entopterygoid; ps, parasphenoid; bsr, branchiostegal ray; cl, cleithrum. (**C**) Quantitative analyses of (B). The length of the ps was measured similarly to Fig. 3E. The data were analyzed by one-way ANOVA with Turkey's test. Statistical significance, *$p < 0.05$; **$p < 0.01$. Error bars indicate s.e.m. Scale bar, 200 μm.

References

Asakawa,K., Suster,M.L., Mizusawa,K., Nagayoshi,S., Kotani,T., Urasaki,A., Kishimoto,Y., Hibi,M., and Kawakami,K. (2008). Genetic dissection of neural circuits by Tol2 transposon-mediated Gal4 gene and enhancer trapping in zebrafish. *Proc. Natl. Acad. Sci. U. S. A* **105,** 1255-1260.

Cermak,T., Doyle,E.L., Christian,M., Wang,L., Zhang,Y., Schmidt,C., Baller,J.A., Somia,N.V., Bogdanove,A.J., and Voytas,D.F. (2011). Efficient design and assembly of custom TALEN and other TAL effector-based constructs for DNA targeting. *Nucleic Acids Res.* **39,** e82.

Distel,M., Wullimann,M.F., and Koster,R.W. (2009). Optimized Gal4 genetics for permanent gene expression mapping in zebrafish. *Proc. Natl. Acad. Sci. U. S. A* **106,** 13365-13370.

Doyle,E.L., Booher,N.J., Standage,D.S., Voytas,D.F., Brendel,V.P., Vandyk,J.K., and Bogdanove,A.J. (2012). TAL Effector-Nucleotide Targeter (TALE-NT) 2.0: tools for TAL effector design and target prediction. *Nucleic Acids Res.* **40,** W117-W122.

Fukui,H., Terai,K., Nakajima,H., Chiba,A., Fukuhara,S., and Mochizuki,N. (2014). S1P-Yap1 signaling regulates endoderm formation required for cardiac precursor cell migration in zebrafish. *Dev. Cell* **31**, 128-136.

Halloran,M.C., Sato-Maeda,M., Warren,J.T., Su,F., Lele,Z., Krone,P.H., Kuwada,J.Y., and Shoji,W. (2000). Laser-induced gene expression in specific cells of transgenic zebrafish. *Development* **127,** 1953-1960.

Kashiwada,T., Fukuhara,S., Terai,K., Tanaka,T., Wakayama,Y., Ando,K., Nakajima,H., Fukui,H., Yuge,S., Saito,Y. et al. (2015). beta-catenin-dependent transcription is central to Bmp-mediated formation of venous vessels. *Development* **142**, 497-509.

Kawakami,K., Takeda,H., Kawakami,N., Kobayashi,M., Matsuda,N., and Mishina,M. (2004). A transposon-mediated gene trap approach identifies developmentally regulated genes in zebrafish. *Dev. Cell* **7**, 133-144.

Kimmel,C.B., Ballard,W.W., Kimmel,S.R., Ullmann,B., and Schilling,T.F. (1995). Stages of embryonic development of the zebrafish. *Dev. Dyn.* **203**, 253-310.

Knopf,F., Hammond,C., Chekuru,A., Kurth,T., Hans,S., Weber,C.W., Mahatma,G., Fisher,S., Brand,M., Schulte-Merker,S. et al. (2011). Bone

regenerates via dedifferentiation of osteoblasts in the zebrafish fin. *Dev. Cell* **20**, 713-724.

Kurita,R., Sagara,H., Aoki,Y., Link,B.A., Arai,K., and Watanabe,S. (2003). Suppression of lens growth by alphaA-crystallin promoter-driven expression of diphtheria toxin results in disruption of retinal cell organization in zebrafish. *Dev. Biol.* **255**, 113-127.

Spoorendonk,K.M., Peterson-Maduro,J., Renn,J., Trowe,T., Kranenbarg,S., Winkler,C., and Schulte-Merker,S. (2008). Retinoic acid and Cyp26b1 are critical regulators of osteogenesis in the axial skeleton. *Development* **135**, 3765-3774.

Uemura,M., Nagasawa,A., and Terai,K. (2016). Yap/Taz transcriptional activity in endothelial cells promotes intramembranous ossification via the BMP pathway. *Sci. Rep.* **6**, 27473.

Urasaki,A., Morvan,G., and Kawakami,K. (2006). Functional dissection of the Tol2 transposable element identified the minimal cis-sequence and a highly repetitive sequence in the subterminal region essential for transposition. *Genetics* **174**, 639-649.

Supplementary movie 1. Video image of a beating heart of *Tg(myl7:NLS-mCherry)* larva at 72 hpf obtained by a light sheet microscope.

Supplementary movie 2. Video image of a beating heart of *Tg(myl7:actn2-tdEos)* larva at 72 hpf obtained by a light sheet microscope.

Supplementary movie 3. Video image of a beating heart of larva injected with control MO at 5 dpf obtained by a stereo microscope. Ventral view, anterior to the left. Scale bar, 125 μm.

Supplementary movie 4. Video image of a beating heart of larva injected with *ostn* MO at 5 dpf obtained by a stereo microscope. Ventral view, anterior to the left. Scale bar, 125 μm.